

UNCLASSIFIED

AD 403 653

*Reproduced
by the*

DEFENSE DOCUMENTATION CENTER

FOR

SCIENTIFIC AND TECHNICAL INFORMATION

CAMERON STATION, ALEXANDRIA, VIRGINIA



UNCLASSIFIED

NOTICE: When government or other drawings, specifications or other data are used for any purpose other than in connection with a definitely related government procurement operation, the U. S. Government thereby incurs no responsibility, nor any obligation whatsoever; and the fact that the Government may have formulated, furnished, or in any way supplied the said drawings, specifications, or other data is not to be regarded by implication or otherwise as in any manner licensing the holder or any other person or corporation, or conveying any rights or permission to manufacture, use or sell any patented invention that may in any way be related thereto.

MASSACHUSETTS INSTITUTE OF TECHNOLOGY

LINCOLN LABORATORY

46 G-2

THE SURFACE RESISTANCE OF HIGH-CURRENT MICROWAVE DISCHARGES IN ARGON

C. E. Muehe

T. J. Fessenden

20 March 1963

The work reported in this document was performed at Lincoln Laboratory, a center for research operated by Massachusetts Institute of Technology. This research is a part of Project DEFENDER, which is sponsored by the U.S. Advanced Research Projects Agency of the Department of Defense; it is supported by ARPA under Air Force Contract AF 19(628)-500 (ARPA Order 85).

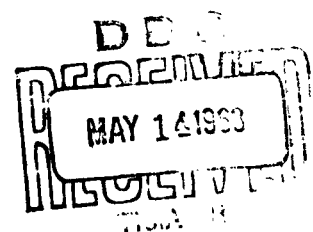
LEXINGTON

MASSACHUSETTS

403 653

When issued, this document had not been reviewed or released for public dissemination by the appropriate government agency. Reproduction or distribution for official government use is authorized. Other reproduction or distribution requires written authorization by Lincoln Laboratory Publications Office.

Upon notification of release, this page may be removed.



ABSTRACT

A digital computer has been used to determine the electric and magnetic fields in an argon plasma with sufficient electron density so that the applied microwave fields are shielded from the interior of the discharge by the skin effect. An approximate method of determining the surface resistance, not requiring a computer, is also given. Some experimental results confirming the theory are presented.

AFESD - TDR - 63-50

THE SURFACE RESISTANCE OF HIGH-CURRENT MICROWAVE DISCHARGES IN ARGON

By

C. E. Muehe and T. J. Fessenden

The duplexer work at Lincoln Laboratory is aimed principally at designing duplexers for extremely high-power radars. The main limitation in power-handling ability of a gas tube duplexer is the heat generated in the switching TR tube (i. e., the one closest to the transmitter). This tube must short the receiver line so that the high power will be directed to the antenna and then must de-ionize quickly after the transmitter pulse so that received signals may enter the receiver.² The switching TR tube consists of a container of easily ionizable gas mounted in a window in the waveguide wall.³ During the transmitter pulse the gas ionizes to such a degree that it is closer to a poorly conducting metal than a lossy dielectric. Thus it always presents a low impedance compared to the impedance of the circuit driving current through it. The first prerequisite in designing such a tube is a knowledge of the heat generated by the current forced through the tube, and to this end a good theoretical understanding of the the plasma within the tube is essential.

Several authors^{2,4} have suggested that conditions existing in a high-frequency discharge should be identical to those existing in the positive column of a d.c. discharge, except that the sustaining field is now a high-frequency electric field instead of a d.c. field. Indeed, several experimenters^{5,6,7} applied first d.c. and then RF fields to the same positive column and found that the rms value of the RF field equalled the d.c. field for equal brightness of the discharge. All of their experiments used

relatively low current densities, frequencies lower than 170 Mcps, and pressures such that the collision frequency of electrons with the gas molecules was higher than the applied frequency. The purpose of the present investigation is to work out a theory to describe cases where the current and frequency are high enough to produce a plasma which, by virtue of its high conductivity, can actually shield the electric field from its interior by the skin effect. Also, we wish to extend the theory to cases where the collision frequency is comparable to or lower than the applied frequency.

In our theoretical investigation, instead of considering a round tube as used in most d.c. positive-column experiments, we will consider the discharge to exist between two sheets of dielectric. (See Fig. 1.) This is a simpler case mathematically besides approaching more nearly the geometry of many microwave discharges (i. e., the discharge behind windows in TR cells^{1,2}). Energy to sustain the discharge is provided by an electromagnetic wave, incident from the left, whose direction of propagation is perpendicular to the dielectric sheets. Most of this incident wave is reflected and, for high-current densities, the electric field is attenuated through the discharge by the skin effect⁸ so that the electric field is lower at the right dielectric boundary ($x = 0$) than at the left.

List of Symbols

Because of the large number of symbols used it has been thought advisable to give below a list of the symbols used, together with their meanings. All equations are in the rationalized M.K.S. system of units, except where the symbols p(mm Hg) or T_e , u , u_1 , u_e (electron volts) occur. The units used on tables and graphs are clearly labeled.

LIST OF SYMBOLS

a	radius of experimental discharge tube
A	surface area of discharge
c	velocity of light
d	spacing between dielectric plates (see Fig. 1)
D_a	ambipolar diffusion coefficient
e	electronic charge
e	base of naperian system of logarithms
\dot{E}	complex a.c. electric field (r.m.s. value)
E	magnitude of the complex electric field (r.m.s. value) or d.c. electric field
E_r	component of electric field in phase with current (r.m.s. value)
\dot{E}_0	complex a.c. electric field at surface (r.m.s. value)
f	applied frequency
$f(u)$	electron distribution function (see Eq. A1)
h_1	proportionality constant for P_1
h_e	proportionality constant for P_e
\dot{H}	complex a.c. magnetic field (r.m.s. value)
\dot{H}_0	complex a.c. magnetic field at surface (r.m.s. value)
H^*	the conjugate value of H
I_0	the short-circuit current at the end of a transmission line
j	$\sqrt{-1}$
J	surface current density
J_1	surface current density at one point of discharge
k_1, k_2	constants
m	electronic mass

LIST OF SYMBOLS, con't.

m	exponent of $\sin \phi$ (See Table I.)
m_p	mass of positive ion
M	mass of gas molecules
n	electron density
n	exponent of J (See Eq. 20)
p	pressure (mm Hg)
P_d	power dissipation in the discharge
P_l	power in the incident wave on a transmission line
P_i	probability of ionization
P_e	probability of excitation
P_c	probability of collision
R	surface resistance of the discharge
R_l	surface resistance at point on discharge where $J = J_l$
S	normalized pointing vector
S	voltage standing wave ratio
T_e	electron temperature in volts ($11,600^\circ K = 1$ volt)
u	electron energy in volts
u_i	ionization potential
u_e	excitation potential
v	velocity
W_c, W_e, W_i	power loss per unit volume for elastic, excitation and ionization losses
W	total power loss per unit volume
x	normalized distance in plasma ($x = pz$)
X	surface reactance of discharge
z	distance into discharge

LIST OF SYMBOLS, con't.

z	distance along axis of experimental tube (Eq. 20)
\dot{Z}	surface impedance of discharge
Z_0	characteristic impedance of transmission line
α	phase angle of the complex electric field
α	real part of propagation constant (See Eq. 24)
β	imaginary part of propagation constant (See Eq. 24)
$\dot{\gamma}$	propagation constant
δ	skin depth
ϵ_0	permittivity of free space
η	normalized charge density
θ	derivative of the phase angle α with respect to x
λ	free space wavelength at the applied frequency
λ_1	wavelength in dielectric
Λ	diffusion length in plasma
$\dot{\mu} = \mu_1 + j\mu_2$	mobility of the electrons
μ_0	permeability of free space
μ_3	positive ion mobility
ν_1	ionization frequency
ν_a	attachment frequency
ν_c	electron collision frequency
ν_{cl}	electron collision frequency at 1 mm Hg
σ	magnitude of the complex conductivity
$\dot{\sigma} = \sigma_1 + j\sigma_2$	complex conductivity of the plasma
$\phi, \phi_1, \phi_2, \phi_3$	angles of a sine curve of current density along a discharge
\oint	limit of integral (See Table I.)
ψ	normalized electric field (E/p)
ω	applied radian frequency

Equations Describing Conditions in the Discharge

For a steady-state discharge using the coordinates of Fig. 1, the electron production and loss rates are related by:⁹

$$(v_i - v_a) n + \frac{d^2(D_a n)}{dz^2} = 0 \quad (1)$$

Here we have assumed that volume recombination between electrons and positive ions is negligible and that conditions are such as to be in the ambipolar-diffusion region. We will also set $v_a = 0$, since we are dealing with an inert gas. The conditions^{10,11} required are that the electron mean-free path, the positive-ion mean-free path, and the thickness of the positive-ion sheath at the walls, all be small compared to both the spacing between the dielectrics d and the skin depth in the plasma.

The variation of electric and magnetic fields (assumed oriented as in Fig. 1) are described by Maxwell's equations⁸ which, for the one-dimensional case, become:

$$-\frac{d\dot{H}}{dz} = \dot{\sigma}\dot{E} + j\omega\epsilon_0\dot{E}, \quad (2)$$

$$\frac{d\dot{E}}{dz} = -j\omega\mu_0\dot{H}. \quad (3)$$

We will assume that $\sigma \gg \omega\epsilon_0$ over most of the discharge and so will drop the last term in Eq. (2). Differentiating (3) and eliminating \dot{H} between (2) and (3), we obtain:

$$\frac{d^2\dot{E}}{dz^2} = j\omega\mu_0\dot{\sigma}\dot{E}, \quad (4)$$

which is the usual skin-effect equation for \dot{E} , except now the conductivity $\dot{\sigma}$ is complex and varies with distance.

Since the electron temperature, conductivity and ionization frequency are all functions of the magnitude of the electric field (see Appendix), let

$$\dot{E} = E e^{j\alpha}, \quad (5)$$

Substituting into Eq. (4) and dividing into real and imaginary parts, we obtain two equations:

$$E \frac{d^2 \alpha}{dz^2} + 2 \frac{dE}{dz} \frac{d\alpha}{dz} = \omega \mu_0 n e \mu_1 E, \quad (6)$$

$$- E \left(\frac{d\alpha}{dz} \right)^2 + \frac{d^2 E}{dz^2} = - \omega \mu_0 n e \mu_2 E, \quad (7)$$

where $\dot{\sigma} = n e \mu_1 + j n e \mu_2$.

Normalizing the Equations

Equations (1), (6) and (7) must be solved using the proper boundary conditions. Before doing this, let us normalize the variables in the following manner. Let $\psi = E/P$; $x = pz$; $\theta = d\alpha/dx$ and $\eta = \frac{\omega \mu_0 n e T_e}{p^3}$. Substituting into (1), (6) and (7), we obtain

$$\left(\frac{v_1}{D_a P^2} \right) + \frac{d^2 \eta}{dx^2} = 0 \quad (8)$$

$$\psi \frac{d\theta}{dx} + 2 \frac{d\psi}{dx} \theta = \left(\frac{\mu_1 P}{T_e} \right) \eta \psi \quad (9)$$

$$- \psi \theta^2 + \frac{d^2 \psi}{dx^2} = - \left(\frac{\mu_2 P}{T_e} \right) \eta \psi \quad (10)$$

In the Appendix it is shown that each of the quantities in parenthesis in Eqs. (8), (9) and (10) is only a function of the electron

temperature and $p\lambda$ for a particular gas and an assumed energy distribution, in this case Maxwellian. These three coefficients have been calculated for argon and are shown as a function of electron temperature in Figs. 2, 3 and 4. Next, an energy balance can be made and the electric field needed to raise a small volume of the plasma to any particular electron temperature determined. The electric field for argon is shown in Fig. 5. When the problem is worked on an electronic computer, a value of $p\lambda$ is chosen and the quantities shown in Figs. 2-5 are computed for many different electron temperatures using the formulas in the Appendix. The answers are stored in a table in the storage of the computer. Then, Eqs. (8)-(10) are solved numerically (subject to certain boundary conditions), and during the solution interpolation in the table of values in the computer memory gives each term in parenthesis in (8) to (10) from the value of ψ at each point in the solution.

Boundary Conditions

The solution to Eqs. (8), (9) and (10) involves the specification of five boundary conditions. Two boundary conditions are given by specifying the impedance (\dot{E}/\dot{H}) presented to an electromagnetic wave leaving from the right of the discharge region. To obtain this impedance, replace \dot{E} in Eq. (3) by $\dot{E}e^{j\alpha}$ and perform the indicated differentiation. This yields:

$$-j\omega\mu_0\dot{H} = \dot{E} \left(\frac{1}{E} \frac{dE}{dz} + j \frac{d\alpha}{dz} \right). \quad (11)$$

Putting into normalized form, the impedance at any point in the discharge is:

$$\frac{\dot{Z}_p}{\omega\mu_0} = - \frac{\dot{E}}{\dot{H}} \frac{p}{\omega\mu_0} = \frac{1}{\theta - j \frac{1}{\psi} \frac{d\psi}{dx}} \quad (12)$$

Notice that \dot{Z} is taken as the negative of the ratio of \dot{E} to \dot{H} . This is a result of the fact that power is flowing from the left to the right, whereas we have purposely taken the positive x direction to the left. At $x = 0$, in Fig. 1, we will present an infinite impedance to the wave exiting from the discharge. This may be done by placing a shorting plane a quarter wavelength to the right of the $x = 0$ point. An infinite impedance requires both the real and imaginary parts of the denominator of (12) to vanish so that θ and $d\psi/dx$ are zero at $x = 0$. Since the tangential E and H must be equal across the boundary at $x = 0$, then these quantities must also be zero just to the left of $x = 0$.

Two other boundary conditions are that $\eta = 0$ at $x = 0$ and at $x = d$. (See Fig. 1.) The last boundary condition is that E have some value at one of the two boundaries. All of the boundary conditions can be made to apply at $x = 0$, except the condition $\eta = 0$ at $x = d$.

The problem can easily be solved as an initial value problem on an electronic computer. To do this we use the following initial conditions at $x = 0$: $\theta = 0$, $d\psi/dx = 0$, $\eta = 0$, $E = E_0$, $d\eta/dx = d\eta/dx|_0$. The computer produces a solution by the usual method of solving simultaneous differential equations and completes its solution when η crosses zero (at which point $x = pd$).

Discussion of Computer Results

Figure 6 shows typical results for a fairly well-shielded case. From (11) and the definition of the normalized variables we obtain for the normalized power flow:

$$S = \frac{-\omega\mu_0}{p^3} \operatorname{Re}(\dot{E} \dot{H}^*) = \psi^2 \theta \quad (13)$$

Taking the derivative of (13) and using (9),

$$\frac{dS}{dx} = \left(\frac{\mu_1 p}{T_e}\right) \eta \psi^2 \quad (14)$$

This equation could have been used instead of (9) in the machine computation. The quantity dS/dx plotted in Fig. 6 is thus the normalized power dissipation per unit depth in the discharge. It is interesting to note that the peak in the power dissipation curve occurs closer to the front window than the peak in the normalized charge density η . Since most of the energy is lost due to exciting collisions, the light from the discharge appears most intense just behind the front window.

A similar graph for sufficiently small $d\tau/dx]_0$ shows no variation of the normalized electric field, ψ across the discharge. Also, η and dS/dx have the shape of the first loop of a sine curve with $d = \pi\sqrt{D_a/v_1}$.

To compare with experimental data we need to know the various quantities at the input to the discharge or at $x = pd$. The surface current density, J , is equal to the magnitude of H , which from (11) is,

$$\frac{J_{\text{ax}}]_0}{p} = \sqrt{\left(\frac{d\psi}{dx}\right)^2 + (\psi\theta)^2}. \quad (15)$$

The surface resistance is the real part of the Eq. (12).

$$\frac{R_p}{\omega\mu_0} = \frac{\theta}{\theta^2 + \left(\frac{1}{\psi} \frac{d\psi}{dx}\right)^2} \quad (16)$$

The normalized surface resistance is plotted as a function of normalized linear current density for an infinite $p\lambda$ in Fig. 7. The set of lines of minus 45 degrees slope for various values of pd represent the unshielded case where the electric field is constant throughout the discharge. All of these lines are asymptotic to a single curve which depicts the well-shielded case. For the well-shielded case the surface resistance

is independent of the spacing d .

For each value of $p\lambda$ we could plot a graph similar to Fig. 7, but this would necessitate a large number of graphs. Instead, we have chosen to present the computed results for the unshielded case (E/P is independent of J) in Fig. 8 and the well-shielded case (R independent of d) in Fig. 9.

The real part of the electric field, E_r , (i.e., the component in phase with the current) is plotted as a function of pd in Fig. 8. It is interesting to note that the curves are displaced from one another by only a factor of about two. It is easy to show that if the collision frequency in the gas were a constant, independent of energy, all the curves in Fig. 8 would fall on top of one another. The approximate mean-free path limit for electrons is marked by a dashed line. Below this limit the electron mean-free path is larger than the diffusion length in the tube. Our theory does not apply below this limit.

In Fig. 9 we have normalized the experimental parameters p and J by multiplying each by the wavelength λ and plotted contours of constant surface resistance. Notice that at a constant current density if the pressure is decreased along some vertical line, the surface resistance slowly decreases until one goes into the "anomalous skin effect" region. The same is true if one holds the pressure constant and increases the current along some horizontal line in Fig. 9. In the "anomalous skin effect" region the mean-free path of electrons in the plasma is greater than the skin depth so that an electron is in a varying electric field over its free path and one cannot specify a unique conductivity for each point in the plasma. This effect has been studied extensively in metals.¹² Our computations do not apply in this region. Also plotted on Fig. 9 is a curve for $X = 30$. To the left of this curve the surface reactance X

is so large that the fields on the outside of the plasma may not be computed on the basis of a zero surface impedance for the plasma.

Electron-Positive Ion Collisions

In the foregoing analysis we have assumed that the only important collisions are the electron-electron and the electron-neutral molecule collisions. However, when the gas has greater than about one percent ionization, the electron-positive ion collision frequency becomes greater than the electron-neutral molecule collision frequency. For the case where ν_c is already large compared to ω , the conductivity will approach a value almost independent of charge density--that of a fully ionized gas:¹³

$$\sigma = 0.582 \left(\frac{2\pi}{em}\right)^{1/2} \frac{64e_o^2 T_e^{3/2}}{\ln \left[\frac{12\pi}{n^{1/2}} \left(\frac{e_o T_e}{e}\right)^{3/2} \right]} \quad (17)$$

The log term varies very slowly with charge density so that only a rough estimate of n need be made. To facilitate computation, contours of constant surface electron temperature have been plotted on Fig. 9 so that one can calculate the approximate surface resistance of a fully ionized plasma.

$$R = \sqrt{\frac{\pi f \mu_o}{\sigma}} \quad (18)$$

If the resistance so calculated is less than R at the point of interest on Fig. 9, the gas is approaching the fully ionized condition. Even in a fully ionized gas the electron temperature will vary with depth into the discharge. This is another problem which can be solved on an electronic computer. When $\nu_c < \omega$, the ω term in the conductivity equation (A5) will become less important as the degree of ionization goes beyond about 1 percent. We will not treat this case here.

Experimental Verification

All of the microwave plasmas considered here have conductivities closer to a metal than a dielectric; therefore, in order to measure the surface resistance they should be incorporated as part of the metallic walls of some microwave circuit. The surface current density is then determined as if the walls were perfect conductors. A calibrated pick-up (probe, loop or directional coupler) is incorporated near the plasma to measure the level of RF current in the plasma. The RF circuit containing the plasma is usually placed at the end of a transmission line on which the incident and reflected waves may be measured to determine the power loss in the plasma. A correction is made to take into account the power loss in the other walls of the microwave circuit, not including the plasma.

The experimental verification of the computed surface resistance is complicated by the fact that it is very difficult to build a microwave circuit such that the surface current densities are uniform in the plasma. There is a variation of current density because: 1) the dimensions of the plasma are not small compared to a wavelength and in most microwave circuits the wall current varies appreciably over a half-wavelength, and 2) since most of the plasmas are of such high intensity that there would be considerable sputtering if metal were not eliminated from areas adjacent to the plasma, some sort of capacitive coupling must be used to conduct the wall currents into and out of the plasma. This capacitive coupling invariably involves a variation of the plasma surface current density in the vicinity of the plasma.

To put these ideas into more concrete form, let us examine a circuit

used by the authors. The tube was mounted at the short-circuited end of a multiple quarter-wavelength stub on a $3\frac{1}{8}$ -inch coaxial line. (See Fig. 10.) A directional coupler measured the power incident on the tube and a slotted line measured the VSWR so that the fraction of the incident power lost in the discharge could be determined. Separate tests, whereby the plasma was replaced by a high-conductivity metal, showed that 0.5 percent of the incident power was lost in the tube mount. At the highest incident power about 4 percent of the incident power was lost so the correction was always small. Six microsecond pulses at a frequency of 425 Mcps were used. The standing wave was viewed with a crystal detector and a well-shielded oscilloscope. A calibrated attenuator was inserted between the pickup probe and the scope. Several filters were used to eliminate extraneous frequencies from the magnetron. It was found that the discharge was well established in about 2 μ sec.

Figure 11 shows in more detail the tube and its mounting. The tube consisted of two pieces of concentric quartz tubing. The annular space between the quartz tubes was filled with spectroscopically pure argon after a thorough bake-out. Two silver bands were baked onto the outside of the tube as shown. A resonant choke was provided to keep the discharge from spreading into the gas reservoir.

RF current on the center conductor is capacitively coupled through the quartz under the silver band at one end, then flows through the plasma and is capacitively coupled out at the other end where it flows through the metal plate shorting the coaxial line. The equivalent circuit of the tube and mount is shown in Fig. 11(b). The current density versus distance along the plasma was calculated using the equivalent circuit and is shown in Fig. 11(c). The current density has been normalized to I_0 (twice the current in the incident wave) at one point on the curve.

To predict the power dissipation in the discharge with the help of Figs. 8 and 9, we first draw a curve of R versus J for the known value of p and λ used in the experiment. (See Fig. 12.) Then the total power dissipation, P_d , is given by

$$P_d = \iint J^2 R dA, \quad (19)$$

where the integration is taken over the surface area of the plasma.

In all cases of interest, J either varies as some part of a sine curve [see Fig. 11(c)] with distance or is a constant. If a constant, the integration of (17) presents no problem. If J varies as a sine function, we presumably know J at one point, J_1 . Let us assume that R varies as J^{-n} ; then $R = R_1 (J/J_1)^{-n}$, where R_1 is the value of R at J_1 and $-n$ is the slope of the R versus J curve (Fig. 12) at the same point. With this approximation, the power dissipated in one section of the tube in Fig. 11 is given by,

$$\begin{aligned} P_d &= \iint J^2 R_1 \left(\frac{J}{J_1}\right)^{-n} dA = 2\pi a \int \frac{R_1}{J_1^{-n}} J^{2-n} dz \\ &= (2\pi a) \left(\frac{\lambda_1}{2\pi}\right) J_1^2 R_1 \int_{\phi_2}^{\phi_3} \left(\frac{\sin \phi}{\sin \phi_1}\right)^{2-n} d\phi \end{aligned} \quad (20)$$

ϕ_1 is the angle on the sine curve where $J = J_1$, ϕ_2 and ϕ_3 are the angles on the sine curve at the ends of the interval being calculated and λ_1 is the wavelength in the region considered. To aid in these calculations, Table I gives the integral of $\sin^m \phi$ from zero to ϕ as a function of ϕ for various values of m . A large number of short-circuit currents, I_o , are assumed and P_d is calculated for each. The equivalent resistance of

the discharge is then P_d/I_o^2 and this resistance equals Z_o/S . We will plot the quantity,

$$\frac{4}{S} = \frac{4P_d}{I_o^2 Z_o}, \quad (21)$$

as a function of $\sqrt{Z_o I_o/2}$ because for all current levels it is a quantity which is directly proportional to some average surface resistance in the discharge; and, where S is high, it is the fraction of the power in the incident wave that is dissipated in the discharge. The results of these computations are shown as the solid curve of Fig. 13.

Experimentally, the VSWR is determined as a function of the incident power. When the standing-wave ratio is not infinite (i. e., the short is somewhat lossy), the short-circuit current, I_o , is not twice the current in the incident wave, but must be corrected for the finite standing-wave ratio. It is easily shown that

$$\frac{I_o \sqrt{Z_o}}{2} = \frac{S}{S+1} \sqrt{P_1}. \quad (22)$$

Unfortunately, we have no other measurements of arc loss in argon microwave discharges where the current density is known to the necessary precision to make the comparison outlined above. Some measurements were made with folded cylinders mounted perpendicular to the axis of the 3 1/8-inch coaxial line. The tube mount is shown in Fig. 14. The incident power was fixed at 250 kw and the pressure was varied. (See Fig. 15.) The current density was very non-uniform, but had a high enough value so that the discharge was well shielded. Referring to Fig. 9, the value of $J\lambda$ was about 600 amperes. If one allows the pressure to vary by moving up and down a vertical line at $J\lambda = 600$, we see that the surface resistance and thus the percent arc loss slowly decrease with decreasing

pressure until at the lowest pressures used, the discharge is well into the "anomalous skin effect" region. At about 0.1 mm Hg the tube would not fire.

Effect of Impurities

It is interesting to note how the material from which the tube is made and the method of processing affect the results. The cold-trapped system consisted of a fore pump and oil diffusion pump which were used to bring the pressure down to approximately 10^{-6} mm Hg. The system was then isolated from the diffusion pump with a glass valve and gas admitted through another glass valve. The pressure was read on either a mercury manometer, a McCloud gauge, or a Dubrovin gauge, depending on the pressure range. The tube was suitably cold-trapped from the rest of the system using liquid nitrogen to maintain as low an impurity content as possible. Each tube was pre-discharged and flushed several times with argon before any readings were taken.

The ultra-high-vacuum system used a diaphragm pressure gauge. The tube and system were baked at 450°C . A vacuum in the 10^{-9} mm of Hg region was achieved before the spectroscopically pure gas was admitted. The system was completely sealed off from high vapor pressure oils or mercury by ultra-high-vacuum metal valves.

The sealed pyrex tube referred to on Fig. 15 was filled on an ultra-high-vacuum system similar to the one described above after a thorough bake-out using spectroscopically pure argon. The tube was run for about 500 hours at 140 amperes current during which time the arc loss varied no more than one percent from the cross shown on Fig. 15. This indicates that the tube had impurities in it and also that either the arc loss is insensitive to the actual level of impurities or that the impurity content stabilized at some fixed value. Dr. R. J. Carbone of Lincoln

Laboratory made measurements using an ultra-high-vacuum system in which known amounts of oxygen were added to the argon. Carbone found that the arc loss is a slowly varying function of the impurity content and the indications were that the cold-trapped system had an impurity content of about one part in a hundred in the pressure range from 1 to 10 mm Hg.

Experience with several pyrex tubes baked and filled on ultra-high vacuum systems and then operated at high-power levels indicated that they all contained considerable impurities. Indeed, some would visibly change color and their temperature would rise to a high value during the first few minutes of operation. This would be followed in the course of an hour or two by a return to a nearly normal color and lower temperature due to clean-up of some of the impurities. The impurity is believed to be mainly water vapor. It is known that pyrex dissolves a large quantity of water in its manufacture. This water slowly diffuses to the surface, diffusing more rapidly if heat is applied. Quartz seems to give up fewer impurities. To overcome this impurity problem in sealed-off tubes a getter may be used. Several tubes using activated uranium getters¹⁴ were filled and sealed off. The results from two are shown on Fig. 15. The one filled at 0.5 mm Hg was allowed to operate for many hours and the gas gradually cleaned up. The original gas pressure could be restored merely by heating the section of the tube where the discharge took place to about 300°C for a few minutes. The pressure variation was determined by the recovery time variation. Notice that all the data for the tubes containing uranium getters lies below that for a very good gas-handling system.

An Approximate Solution to the Well-Shielded Case

We can make a fairly good estimate of the surface resistance in the

well-shielded case if we compare the computed solution to the results which would be obtained if the conductivity of the plasma were constant (i.e., not a function of distance into the plasma). The solution to equation (4), if $\dot{\sigma}$ is constant but complex, is:

$$\dot{E} = \dot{E}_0 e^{\frac{+ \sqrt{j\omega\mu_0 \dot{\sigma}} z}{\sigma}}, \quad (23)$$

so that the propagation constant $\dot{\gamma}$ is

$$\dot{\gamma} = \alpha + j\beta = \sqrt{j\omega\mu_0 \dot{\sigma}}. \quad (24)$$

Separating this equation into real and imaginary parts and solving for α , we obtain

$$\alpha = \frac{1}{\delta} = \sqrt{\frac{\omega\mu_0}{2}} (\sqrt{\sigma_1^2 + \sigma_2^2} - \sigma_2). \quad (25)$$

Combining equations (23) and (3), we find that the surface impedance \dot{Z} is

$$\dot{Z} = R + jX = \sqrt{\frac{j\omega\mu_0}{\dot{\sigma}}}. \quad (26)$$

Separating this equation into real and imaginary parts and solving for R we obtain:

$$R = \sqrt{\frac{\omega\mu_0}{2\sigma}} (\sqrt{\sigma_2^2 + \sigma_1^2} + \sigma_2). \quad (27)$$

Now, if we multiply equation (25) by (27) we obtain

$$R = \pi f \mu_0 \frac{\sigma_1}{\sigma} \delta. \quad (28)$$

Notice that we have eliminated the charge density by the above manipulation since

$$\frac{\sigma_1}{\sigma} = \frac{1}{\sqrt{1 + \left(\frac{\omega}{\nu_c}\right)^2}}, \quad (29)$$

where ν_c must be interpreted as some average collision frequency.

Now, returning to the actual microwave plasma, we note in Fig. 6 that in a well-shielded discharge, because of the high field there, most of the electrons are created near the front wall and diffuse to the front wall. It seems a good approximation to set the diffusion length⁹ Λ equal to some multiple of the distance it takes the electric field to decrease to $1/e$ times its surface value or let

$$\Lambda = k_1 \delta. \quad (30)$$

Now, Eq. (28) does not strictly apply, but it seems a reasonable approximation if the variation of charge density and electric field are of similar shape in all of the well-shielded discharges studied. So, let

$$R = \pi f \mu_0 k_2 \frac{\sigma_1}{\sigma} \delta. \quad (31)$$

By eliminating δ between (30) and (31), we find

$$\frac{Rp}{\omega \mu_0} = \frac{k_2}{k_1} \frac{\sigma_1}{\sigma} \frac{p\Lambda}{2}, \quad (32)$$

and

$$\frac{J_{ax} \mu_0}{p^2} = \frac{E_r}{R} \frac{\omega \mu_0}{p^2} = \frac{2E_r}{p^2 \Lambda} \frac{\sigma}{\sigma_1} \frac{k_1}{k_2} \quad (33)$$

where E_r is the component of electric field in phase with the current. Now we can measure or calculate by the methods of the Appendix E_r/p as a function of $p\Lambda$. (See Fig. 8 and Fig. A2.) For the high-pressure case, where σ_1/σ is one, we have plotted on log-log paper the calculated values of $p\Lambda/2$ versus $2E_r/p^2\Lambda$ and compared the curve with the well-shielded curve of Fig. 7 and find that by shifting the curve of Fig. 7 downward and to the right a factor of 0.61, the two curves could be made to coincide to within 10 percent over their entire length ($k_1/k_2 = 0.61$). If we assume $k_2 = 1$, we may interpret this result as suggesting that the diffusion length Λ is 0.61 times the skin depth, a not unreasonable suggestion.

If we can assume a constant collision frequency, we may also plot an approximate graph similar to Fig. 9. First, using equations (29) and (33), we find

$$J\lambda = \left(\frac{2k_1}{\mu_0 k_2}\right) \left(\frac{E_r}{p^2\Lambda}\right) p\lambda \sqrt{\left(\frac{p\lambda}{2\pi c}\right)^2 + \frac{1}{v_{c1}^2}} \quad (34)$$

As pointed out previously, if the collision frequency is constant, there is a single curve of E_r/p versus $p\Lambda$ and this curve can be determined from dc measurements on a positive column. Choosing various values of $p\Lambda$ and their corresponding values of E_r/p , we may calculate and plot curves of $J\lambda$ versus $p\lambda$. They will have nearly the same shape as the constant T_e curves of Fig. 9. because, for a diffusion-controlled discharge, there is a unique electron temperature for each $p\Lambda$. Finally, Eq. (32) gives

$$p\lambda = 2\pi c \sqrt{\left(\frac{p\lambda}{R} \frac{k_2 \mu_0}{2k_1}\right)^2 - \frac{1}{v_{c1}^2}} \quad (35)$$

The value of $p\lambda$ can now be found for a fixed value of R and various values of $p\Lambda$ and the constant R curves plotted.

Since in many gases $E\Lambda$ is approximately a constant over wide ranges of $p\lambda$, it is instructive to eliminate $p\lambda$ between equations (32) and (33), giving

$$J\lambda = (E_r\Lambda) \left(\frac{k_2\mu_0}{2k_1} \right) \frac{2\pi c}{\sqrt{1 + \left(\frac{2\pi c}{v_{c1}p\lambda} \right)^2}} \frac{1}{R^2}. \quad (36)$$

From (36) we can see that if $E_r\Lambda$ and v_{c1} were constants, the constant R lines in Fig. 9 would be vertical for large values of $p\lambda$ and approach 45 degree lines for small values of $p\lambda$. This bending for small values of $p\lambda$ is because lowering the value v_c/ω increases the skin depth faster than it lowers the real part of the conductivity. According to Eq. (36), the constant R lines of Fig. 9 bend to the right at high values of $p\lambda$ because $E_r\Lambda$ is increasing rapidly for the values of $p\lambda$ in this region.

Conclusions

The analysis of skin effect in high-density microwave plasmas should aid considerably in predicting the heat loss in gas tube duplexers using argon. The approximate analysis should help where other gases are used and a knowledge of their dc sustaining fields is available. There are several interesting regions left for investigation. More experiments using argon should be performed to compare with the computed results. The experiments should be designed so that the surface-current distribution is known precisely; also, the impurities should be held to the lowest values possible.

Both theoretical and experimental investigations should be made of regions not covered by the present theory. The "anomalous skin effect"

region and the region where the charge density is high enough so that electron-positive ion collisions become important are two examples. Finally, experimentally measured dc sustaining fields and recovery times of positive columns in a variety of gases and gas mixtures, together with the approximate theory worked out in this paper, could be used to easily evaluate these gases for possible use in TR devices.

TABLE I
INTEGRAL OF $\sin \phi$ TO THE m^{th} POWER FROM ZERO TO ϕ

ϕ Degrees	m						
	1.00	1.10	1.20	1.30	1.40	1.50	1.60
0.5000	0.0000	0.0000	0.0000	0.0000	0.0000	0.0000	0.0000
1.0000	0.0002	0.0001	0.0001	0.0000	0.0000	0.0000	0.0000
1.5000	0.0003	0.0002	0.0002	0.0001	0.0001	0.0000	0.0000
2.0000	0.0006	0.0004	0.0003	0.0002	0.0001	0.0000	0.0000
2.5000	0.0010	0.0007	0.0005	0.0003	0.0002	0.0001	0.0001
3.0000	0.0014	0.0010	0.0007	0.0005	0.0003	0.0002	0.0001
3.5000	0.0019	0.0013	0.0010	0.0007	0.0005	0.0003	0.0002
4.0000	0.0024	0.0018	0.0013	0.0010	0.0007	0.0005	0.0003
4.5000	0.0031	0.0023	0.0017	0.0012	0.0009	0.0007	0.0004
5.0000	0.0038	0.0028	0.0021	0.0016	0.0012	0.0009	0.0005
5.5000	0.0046	0.0035	0.0026	0.0020	0.0015	0.0011	0.0007
6.0000	0.0055	0.0042	0.0032	0.0024	0.0019	0.0014	0.0011
6.5000	0.0064	0.0049	0.0038	0.0029	0.0022	0.0017	0.0013
7.0000	0.0075	0.0058	0.0044	0.0034	0.0027	0.0021	0.0016
7.5000	0.0086	0.0066	0.0052	0.0040	0.0032	0.0025	0.0019
8.0000	0.0097	0.0076	0.0060	0.0047	0.0037	0.0029	0.0023
8.5000	0.0110	0.0086	0.0068	0.0054	0.0043	0.0034	0.0027
9.0000	0.0123	0.0097	0.0077	0.0061	0.0049	0.0039	0.0031
9.5000	0.0137	0.0109	0.0087	0.0069	0.0056	0.0045	0.0036
10.0000	0.0152	0.0121	0.0097	0.0078	0.0063	0.0051	0.0041
10.5000	0.0167	0.0135	0.0108	0.0087	0.0071	0.0057	0.0046
11.0000	0.0184	0.0148	0.0120	0.0097	0.0079	0.0064	0.0052
11.5000	0.0201	0.0163	0.0132	0.0108	0.0088	0.0072	0.0059
12.0000	0.0219	0.0178	0.0145	0.0119	0.0097	0.0080	0.0066
12.5000	0.0237	0.0194	0.0159	0.0130	0.0107	0.0088	0.0073
13.0000	0.0256	0.0210	0.0173	0.0143	0.0118	0.0097	0.0081
13.5000	0.0276	0.0228	0.0188	0.0155	0.0129	0.0107	0.0089
14.0000	0.0297	0.0246	0.0203	0.0169	0.0141	0.0117	0.0099
14.5000	0.0319	0.0264	0.0220	0.0183	0.0153	0.0128	0.0107
15.0000	0.0341	0.0284	0.0237	0.0198	0.0166	0.0139	0.0117
15.5000	0.0364	0.0304	0.0254	0.0213	0.0179	0.0151	0.0127
16.0000	0.0387	0.0324	0.0272	0.0229	0.0193	0.0163	0.0138
16.5000	0.0412	0.0346	0.0291	0.0246	0.0208	0.0176	0.0149
17.0000	0.0437	0.0368	0.0311	0.0263	0.0223	0.0189	0.0161
17.5000	0.0463	0.0391	0.0331	0.0281	0.0239	0.0204	0.0174
18.0000	0.0489	0.0415	0.0352	0.0300	0.0256	0.0218	0.0187
18.5000	0.0517	0.0439	0.0374	0.0319	0.0273	0.0234	0.0200
19.0000	0.0545	0.0464	0.0396	0.0339	0.0291	0.0249	0.0215
19.5000	0.0574	0.0490	0.0419	0.0360	0.0309	0.0266	0.0229
20.0000	0.0603	0.0516	0.0443	0.0381	0.0328	0.0283	0.0245
20.5000	0.0633	0.0543	0.0467	0.0403	0.0348	0.0301	0.0261
21.0000	0.0664	0.0571	0.0493	0.0426	0.0368	0.0319	0.0277
21.5000	0.0696	0.0600	0.0518	0.0449	0.0389	0.0338	0.0294
22.0000	0.0728	0.0629	0.0545	0.0473	0.0411	0.0358	0.0312
22.5000	0.0761	0.0659	0.0572	0.0498	0.0434	0.0378	0.0331
23.0000	0.0795	0.0690	0.0600	0.0523	0.0457	0.0399	0.0350
23.5000	0.0829	0.0721	0.0629	0.0549	0.0480	0.0421	0.0370
24.0000	0.0865	0.0753	0.0658	0.0576	0.0505	0.0443	0.0390
24.5000	0.0900	0.0786	0.0688	0.0603	0.0530	0.0466	0.0411
25.0000	0.0937	0.0820	0.0719	0.0631	0.0556	0.0490	0.0433
25.5000	0.0974	0.0854	0.0750	0.0660	0.0582	0.0514	0.0455
26.0000	0.1012	0.0889	0.0782	0.0690	0.0609	0.0539	0.0478
26.5000	0.1051	0.0924	0.0815	0.0720	0.0637	0.0565	0.0502
27.0000	0.1090	0.0961	0.0848	0.0751	0.0666	0.0591	0.0526
27.5000	0.1130	0.0997	0.0883	0.0782	0.0695	0.0618	0.0551
28.0000	0.1171	0.1035	0.0917	0.0815	0.0725	0.0646	0.0577
28.5000	0.1212	0.1073	0.0953	0.0848	0.0755	0.0674	0.0603
29.0000	0.1254	0.1112	0.0989	0.0881	0.0787	0.0704	0.0630
29.5000	0.1296	0.1152	0.1026	0.0916	0.0819	0.0733	0.0658
30.0000	0.1340	0.1193	0.1064	0.0951	0.0852	0.0764	0.0686
30.5000	0.1384	0.1234	0.1102	0.0987	0.0885	0.0795	0.0715
31.0000	0.1428	0.1275	0.1141	0.1023	0.0919	0.0827	0.0745
31.5000	0.1474	0.1318	0.1181	0.1060	0.0954	0.0860	0.0776
32.0000	0.1520	0.1361	0.1221	0.1098	0.0989	0.0893	0.0807
32.5000	0.1566	0.1405	0.1262	0.1137	0.1026	0.0927	0.0839
33.0000	0.1613	0.1449	0.1304	0.1176	0.1063	0.0962	0.0872
33.5000	0.1661	0.1494	0.1347	0.1216	0.1100	0.0997	0.0905
34.0000	0.1710	0.1540	0.1390	0.1257	0.1139	0.1033	0.0939
34.5000	0.1759	0.1586	0.1433	0.1298	0.1178	0.1070	0.0974
35.0000	0.1808	0.1633	0.1478	0.1340	0.1217	0.1108	0.1009
35.5000	0.1859	0.1681	0.1521	0.1383	0.1258	0.1146	0.1045
36.0000	0.1910	0.1729	0.1569	0.1426	0.1299	0.1185	0.1082
36.5000	0.1961	0.1778	0.1615	0.1470	0.1341	0.1224	0.1120
37.0000	0.2014	0.1828	0.1662	0.1515	0.1383	0.1265	0.1158
37.5000	0.2066	0.1878	0.1710	0.1560	0.1426	0.1306	0.1198
38.0000	0.2120	0.1929	0.1759	0.1607	0.1470	0.1348	0.1237
38.5000	0.2174	0.1980	0.1808	0.1653	0.1515	0.1390	0.1278
39.0000	0.2229	0.2032	0.1857	0.1701	0.1560	0.1433	0.1319
39.5000	0.2284	0.2085	0.1908	0.1749	0.1606	0.1477	0.1361
40.0000	0.2340	0.2138	0.1959	0.1798	0.1653	0.1522	0.1404
40.5000	0.2396	0.2192	0.2010	0.1847	0.1700	0.1567	0.1447
41.0000	0.2453	0.2247	0.2063	0.1897	0.1748	0.1613	0.1491
41.5000	0.2510	0.2302	0.2116	0.1948	0.1797	0.1660	0.1536
42.0000	0.2569	0.2358	0.2169	0.1999	0.1846	0.1708	0.1582
42.5000	0.2627	0.2414	0.2223	0.2052	0.1896	0.1756	0.1628
43.0000	0.2686	0.2471	0.2278	0.2104	0.1947	0.1804	0.1675
43.5000	0.2746	0.2529	0.2334	0.2158	0.1998	0.1854	0.1722
44.0000	0.2807	0.2587	0.2390	0.2212	0.2051	0.1904	0.1771
44.5000	0.2867	0.2646	0.2446	0.2266	0.2103	0.1955	0.1820

TABLE 1 (Continued)

ϕ Degrees	m						
	1.00	1.10	1.20	1.30	1.40	1.50	1.60
45.0000	0.2929	0.2785	0.2584	0.2322	0.2157	0.2007	0.1870
45.5000	0.2991	0.2765	0.2562	0.2378	0.2211	0.2059	0.1920
46.0000	0.3053	0.2826	0.2620	0.2434	0.2265	0.2112	0.1971
46.5000	0.3116	0.2887	0.2679	0.2491	0.2321	0.2165	0.2023
47.0000	0.3180	0.2948	0.2739	0.2549	0.2377	0.2219	0.2076
47.5000	0.3244	0.3010	0.2799	0.2608	0.2433	0.2274	0.2129
48.0000	0.3309	0.3073	0.2860	0.2667	0.2491	0.2330	0.2183
48.5000	0.3374	0.3136	0.2921	0.2726	0.2549	0.2386	0.2237
49.0000	0.3439	0.3200	0.2983	0.2786	0.2607	0.2443	0.2293
49.5000	0.3506	0.3264	0.3046	0.2847	0.2666	0.2501	0.2349
50.0000	0.3572	0.3329	0.3109	0.2909	0.2726	0.2559	0.2405
50.5000	0.3639	0.3394	0.3173	0.2971	0.2786	0.2618	0.2463
51.0000	0.3707	0.3460	0.3237	0.3033	0.2847	0.2677	0.2521
51.5000	0.3775	0.3527	0.3301	0.3096	0.2909	0.2737	0.2579
52.0000	0.3843	0.3594	0.3367	0.3160	0.2971	0.2799	0.2630
52.5000	0.3912	0.3661	0.3433	0.3224	0.3034	0.2859	0.2690
53.0000	0.3982	0.3729	0.3499	0.3289	0.3097	0.2921	0.2759
53.5000	0.4052	0.3797	0.3566	0.3355	0.3161	0.2984	0.2820
54.0000	0.4122	0.3866	0.3633	0.3421	0.3226	0.3047	0.2882
54.5000	0.4193	0.3935	0.3701	0.3487	0.3291	0.3111	0.2945
55.0000	0.4264	0.4005	0.3770	0.3554	0.3357	0.3175	0.3000
55.5000	0.4336	0.4076	0.3839	0.3622	0.3423	0.3240	0.3071
56.0000	0.4408	0.4146	0.3908	0.3690	0.3490	0.3306	0.3136
56.5000	0.4481	0.4218	0.3978	0.3759	0.3557	0.3372	0.3201
57.0000	0.4554	0.4289	0.4048	0.3828	0.3625	0.3439	0.3266
57.5000	0.4627	0.4361	0.4119	0.3898	0.3694	0.3506	0.3332
58.0000	0.4701	0.4434	0.4191	0.3968	0.3763	0.3574	0.3399
58.5000	0.4775	0.4507	0.4262	0.4038	0.3832	0.3642	0.3466
59.0000	0.4850	0.4580	0.4335	0.4110	0.3902	0.3711	0.3534
59.5000	0.4925	0.4654	0.4408	0.4181	0.3973	0.3781	0.3603
60.0000	0.5000	0.4729	0.4481	0.4253	0.4044	0.3851	0.3672
60.5000	0.5076	0.4803	0.4554	0.4326	0.4116	0.3922	0.3742
61.0000	0.5152	0.4878	0.4628	0.4399	0.4188	0.3993	0.3812
61.5000	0.5228	0.4954	0.4703	0.4473	0.4266	0.4064	0.3882
62.0000	0.5305	0.5030	0.4778	0.4547	0.4334	0.4136	0.3954
62.5000	0.5383	0.5106	0.4853	0.4621	0.4407	0.4209	0.4025
63.0000	0.5460	0.5183	0.4929	0.4696	0.4481	0.4282	0.4090
63.5000	0.5538	0.5260	0.5005	0.4771	0.4556	0.4356	0.4170
64.0000	0.5616	0.5337	0.5082	0.4847	0.4630	0.4430	0.4244
64.5000	0.5695	0.5415	0.5159	0.4923	0.4706	0.4505	0.4310
65.0000	0.5774	0.5493	0.5236	0.5000	0.4782	0.4580	0.4392
65.5000	0.5853	0.5572	0.5314	0.5077	0.4858	0.4655	0.4467
66.0000	0.5933	0.5651	0.5392	0.5154	0.4935	0.4731	0.4542
66.5000	0.6013	0.5730	0.5471	0.5232	0.5012	0.4808	0.4610
67.0000	0.6093	0.5809	0.5549	0.5310	0.5089	0.4884	0.4694
67.5000	0.6173	0.5889	0.5629	0.5389	0.5167	0.4962	0.4771
68.0000	0.6254	0.5969	0.5708	0.5468	0.5245	0.5039	0.4848
68.5000	0.6335	0.6050	0.5788	0.5547	0.5324	0.5118	0.4925
69.0000	0.6416	0.6130	0.5868	0.5627	0.5403	0.5196	0.5003
69.5000	0.6498	0.6211	0.5949	0.5707	0.5483	0.5275	0.5082
70.0000	0.6580	0.6293	0.6029	0.5787	0.5562	0.5354	0.5160
70.5000	0.6662	0.6374	0.6111	0.5868	0.5643	0.5434	0.5240
71.0000	0.6744	0.6456	0.6192	0.5948	0.5723	0.5514	0.5319
71.5000	0.6827	0.6539	0.6274	0.6030	0.5804	0.5594	0.5399
72.0000	0.6910	0.6621	0.6356	0.6111	0.5885	0.5675	0.5480
72.5000	0.6993	0.6704	0.6438	0.6193	0.5967	0.5756	0.5560
73.0000	0.7076	0.6787	0.6521	0.6275	0.6049	0.5838	0.5641
73.5000	0.7160	0.6870	0.6604	0.6358	0.6131	0.5919	0.5723
74.0000	0.7244	0.6953	0.6687	0.6441	0.6213	0.6002	0.5804
74.5000	0.7328	0.7037	0.6770	0.6524	0.6296	0.6084	0.5887
75.0000	0.7412	0.7121	0.6854	0.6607	0.6379	0.6167	0.5969
75.5000	0.7496	0.7205	0.6937	0.6691	0.6462	0.6250	0.6052
76.0000	0.7581	0.7289	0.7021	0.6774	0.6546	0.6333	0.6135
76.5000	0.7666	0.7374	0.7106	0.6858	0.6629	0.6416	0.6218
77.0000	0.7750	0.7459	0.7190	0.6943	0.6713	0.6500	0.6302
77.5000	0.7836	0.7543	0.7275	0.7027	0.6798	0.6584	0.6385
78.0000	0.7921	0.7629	0.7360	0.7112	0.6882	0.6669	0.6470
78.5000	0.8006	0.7714	0.7445	0.7197	0.6967	0.6753	0.6554
79.0000	0.8092	0.7799	0.7530	0.7282	0.7052	0.6838	0.6630
79.5000	0.8178	0.7885	0.7616	0.7367	0.7137	0.6923	0.6723
80.0000	0.8264	0.7971	0.7701	0.7453	0.7222	0.7008	0.6808
80.5000	0.8350	0.8056	0.7787	0.7538	0.7308	0.7093	0.6894
81.0000	0.8436	0.8142	0.7873	0.7624	0.7393	0.7179	0.6979
81.5000	0.8522	0.8229	0.7959	0.7710	0.7479	0.7265	0.7065
82.0000	0.8608	0.8315	0.8045	0.7796	0.7565	0.7351	0.7151
82.5000	0.8695	0.8401	0.8131	0.7882	0.7651	0.7437	0.7237
83.0000	0.8781	0.8488	0.8218	0.7969	0.7738	0.7523	0.7323
83.5000	0.8868	0.8574	0.8304	0.8055	0.7824	0.7609	0.7409
84.0000	0.8955	0.8661	0.8391	0.8142	0.7911	0.7696	0.7495
84.5000	0.9042	0.8748	0.8478	0.8228	0.7997	0.7782	0.7582
85.0000	0.9128	0.8835	0.8565	0.8315	0.8084	0.7869	0.7669
85.5000	0.9215	0.8922	0.8651	0.8402	0.8171	0.7956	0.7755
86.0000	0.9302	0.9009	0.8738	0.8489	0.8258	0.8043	0.7842
86.5000	0.9390	0.9096	0.8825	0.8576	0.8345	0.8130	0.7929
87.0000	0.9477	0.9183	0.8913	0.8663	0.8432	0.8217	0.8016
87.5000	0.9564	0.9270	0.9000	0.8750	0.8519	0.8304	0.8103
88.0000	0.9651	0.9357	0.9087	0.8837	0.8606	0.8391	0.8191
88.5000	0.9738	0.9444	0.9174	0.8925	0.8693	0.8478	0.8278
89.0000	0.9825	0.9532	0.9261	0.9012	0.8781	0.8566	0.8365
89.5000	0.9913	0.9619	0.9349	0.9099	0.8868	0.8653	0.8452
90.0000	1.0000	0.9706	0.9436	0.9186	0.8955	0.8740	0.8540

3-46-5890

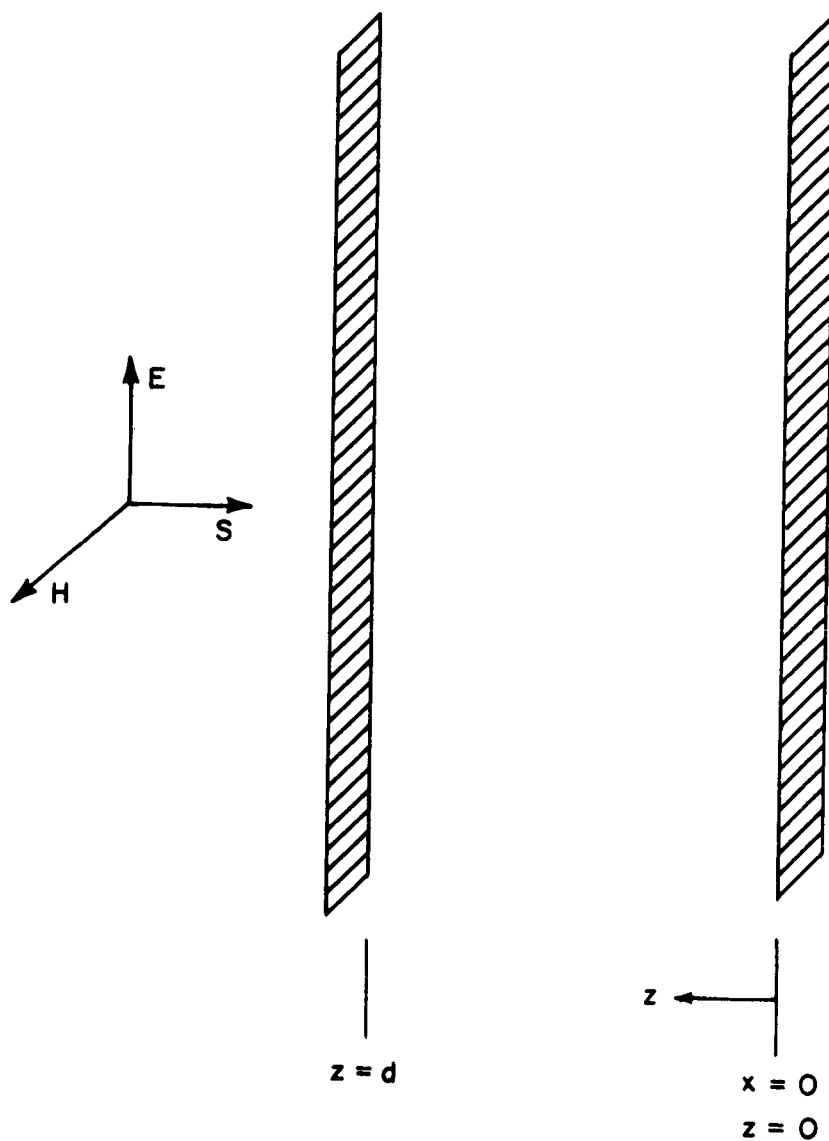


FIG. 1 Geometry of Discharge

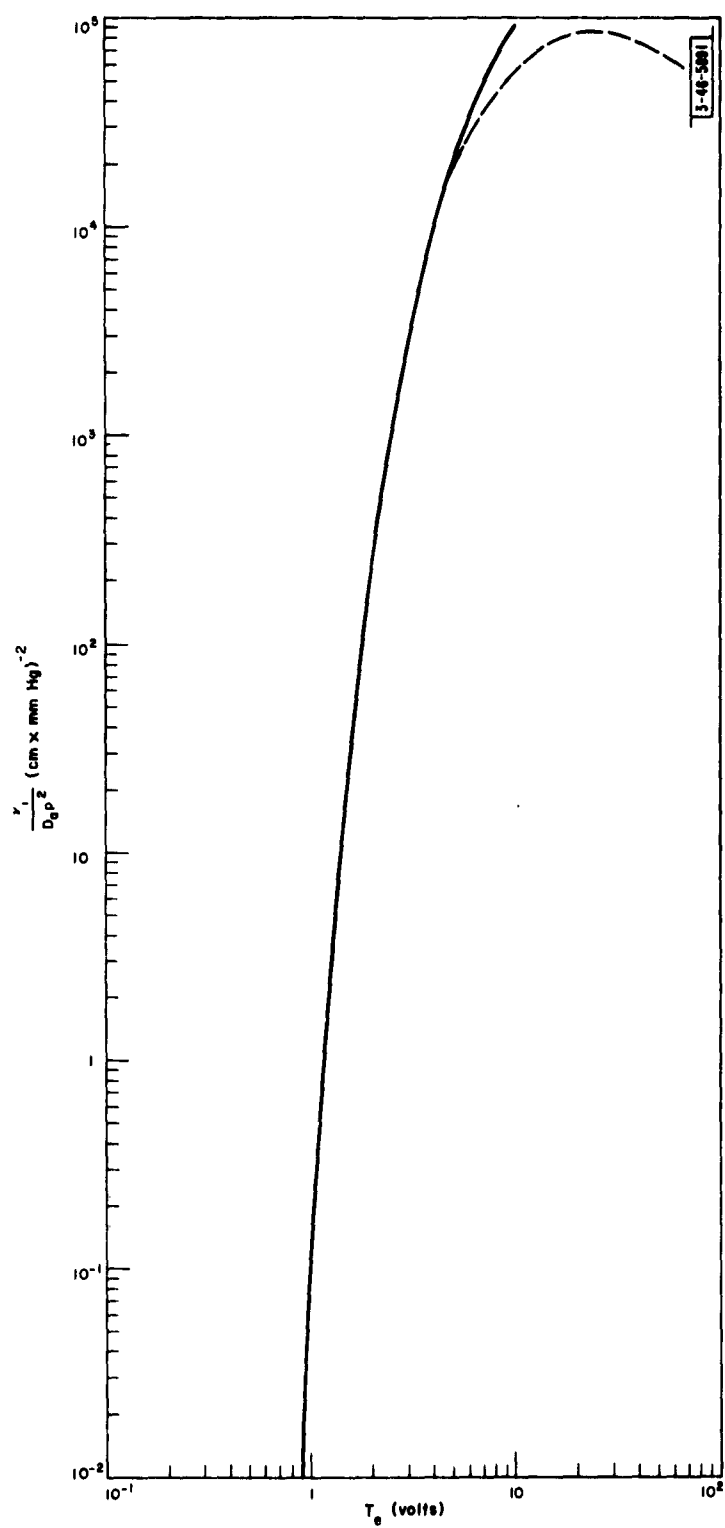


FIG. 2 Ionization Function Versus Electron Temperature for Argon

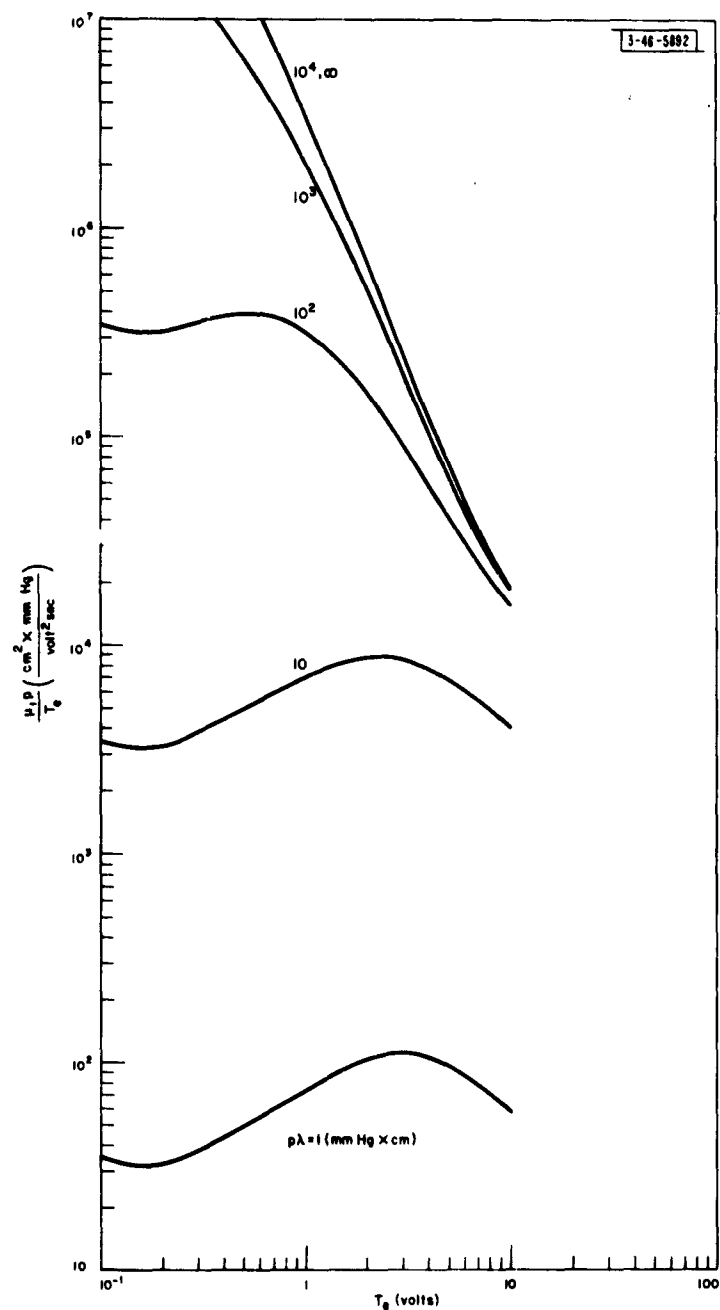


FIG. 3 Real Part of Mobility Versus Electron Temperature in Argon

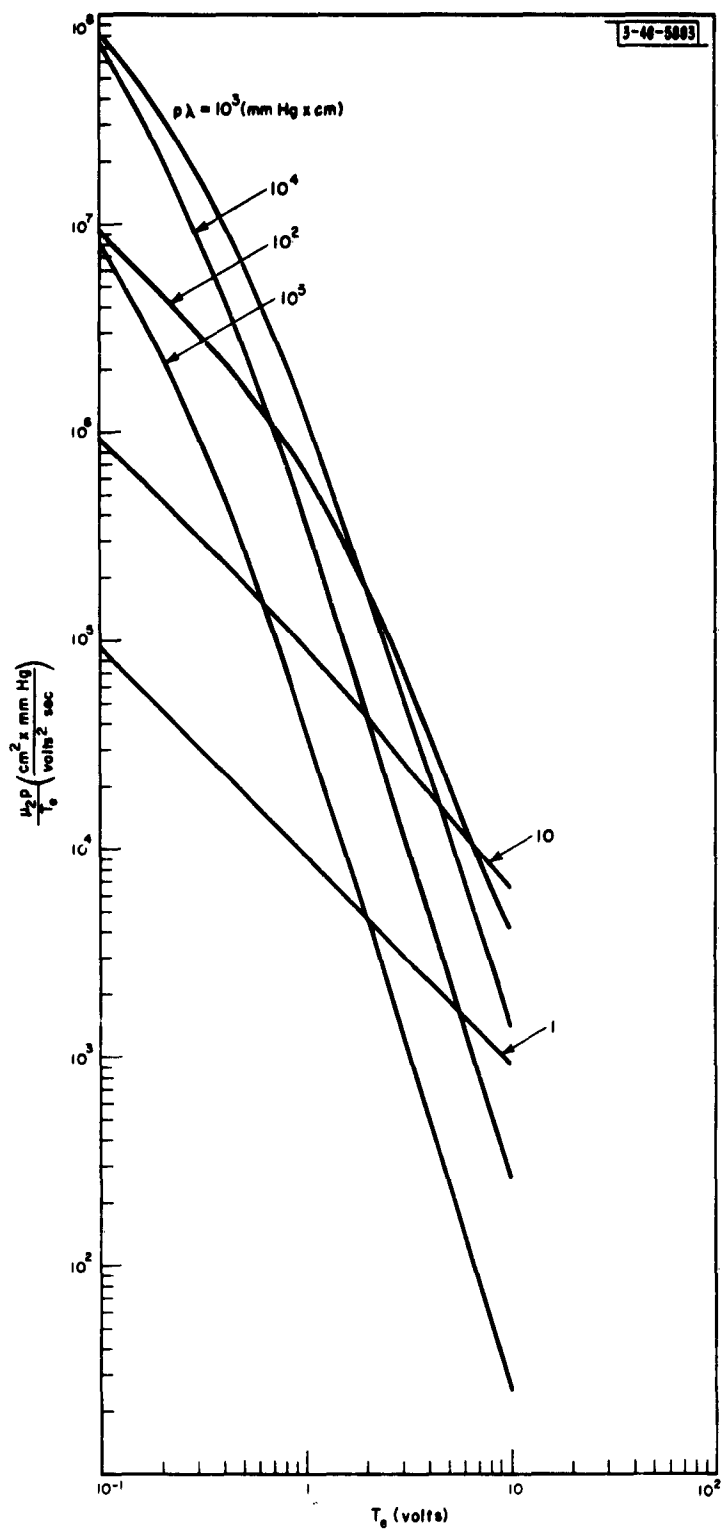


FIG. 4 Imaginary Part of Mobility Versus Electron Temperature for Argon

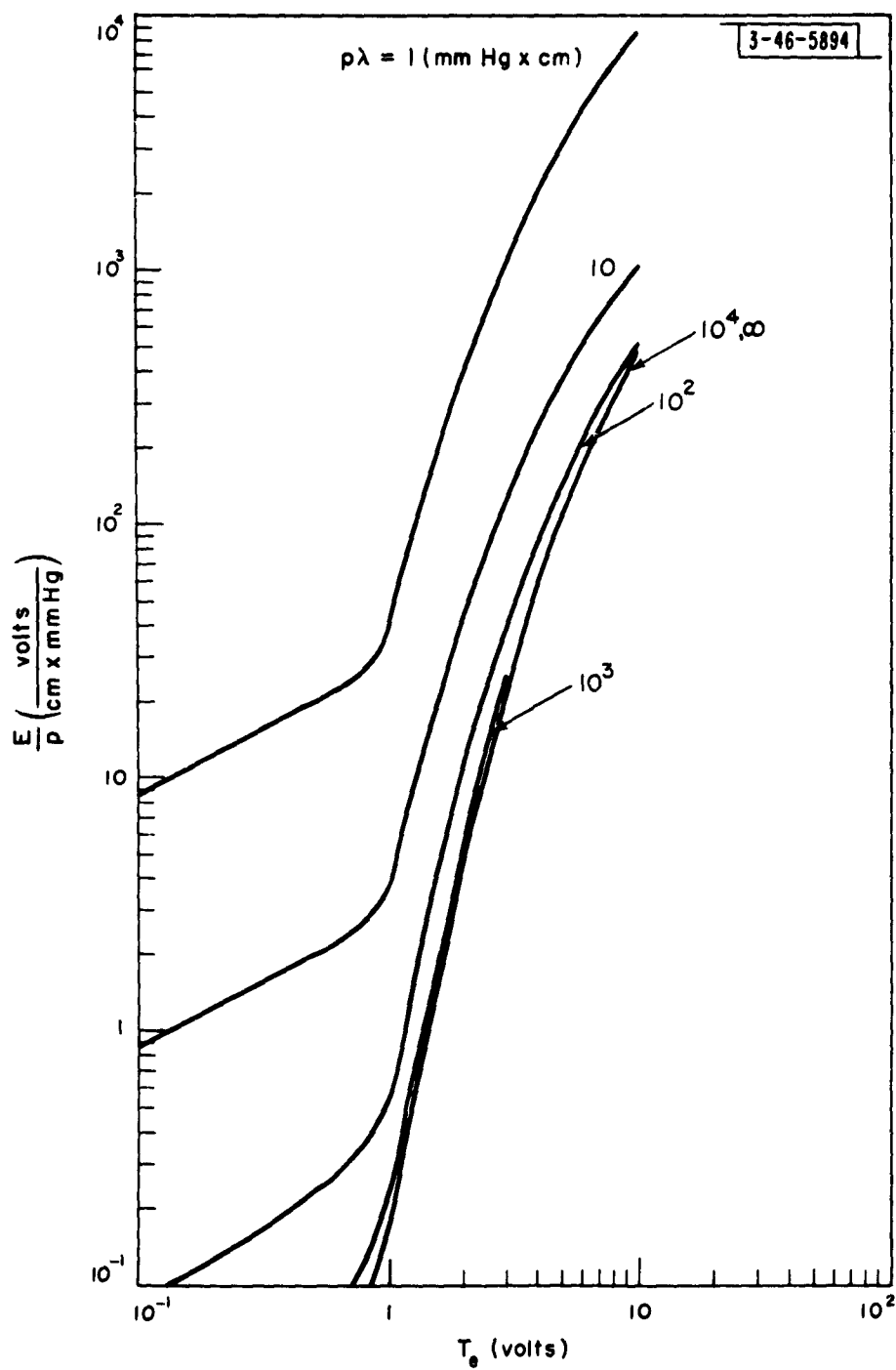


FIG. 5 Electric Field Versus Electron Temperature for Argon

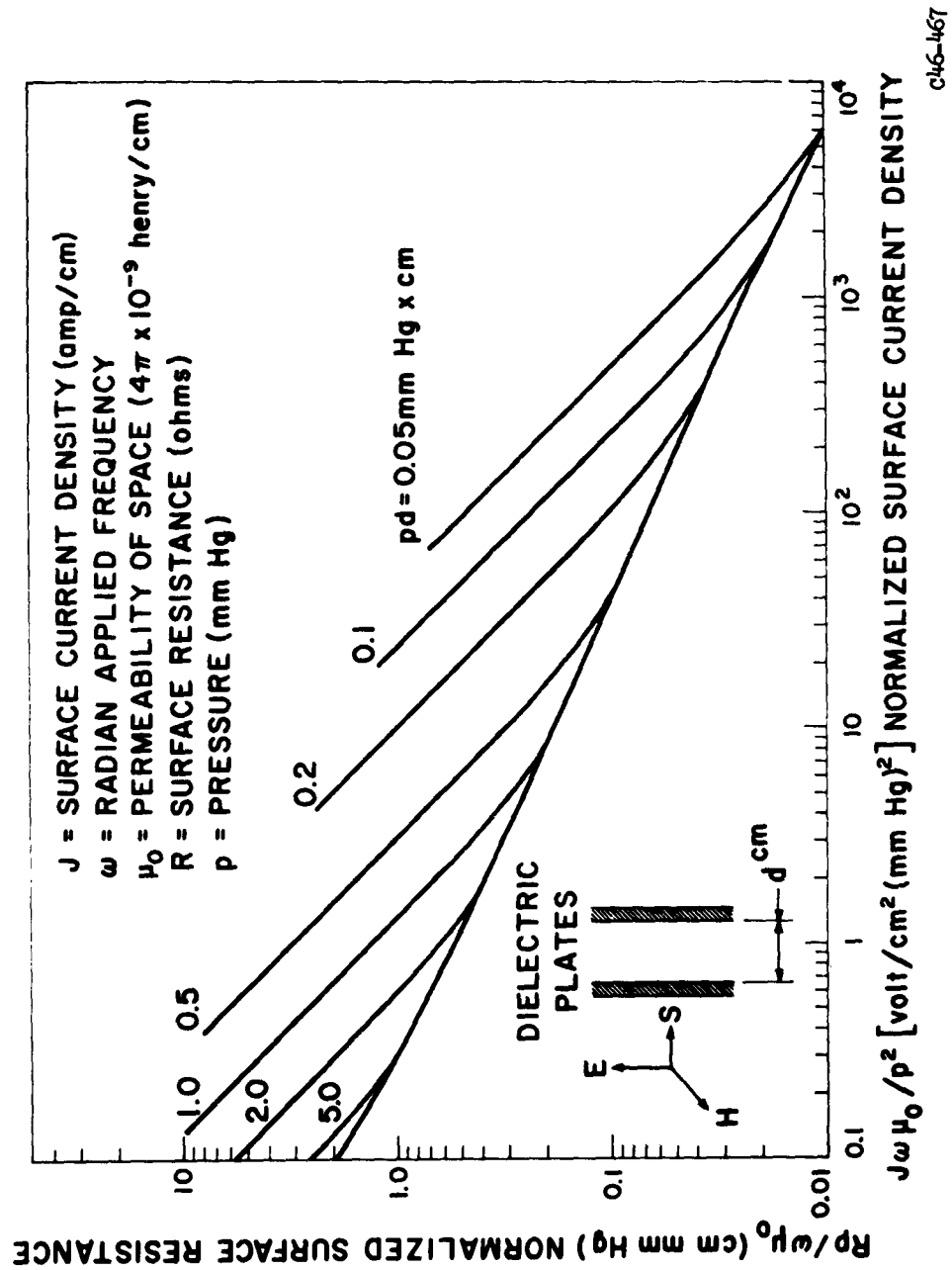
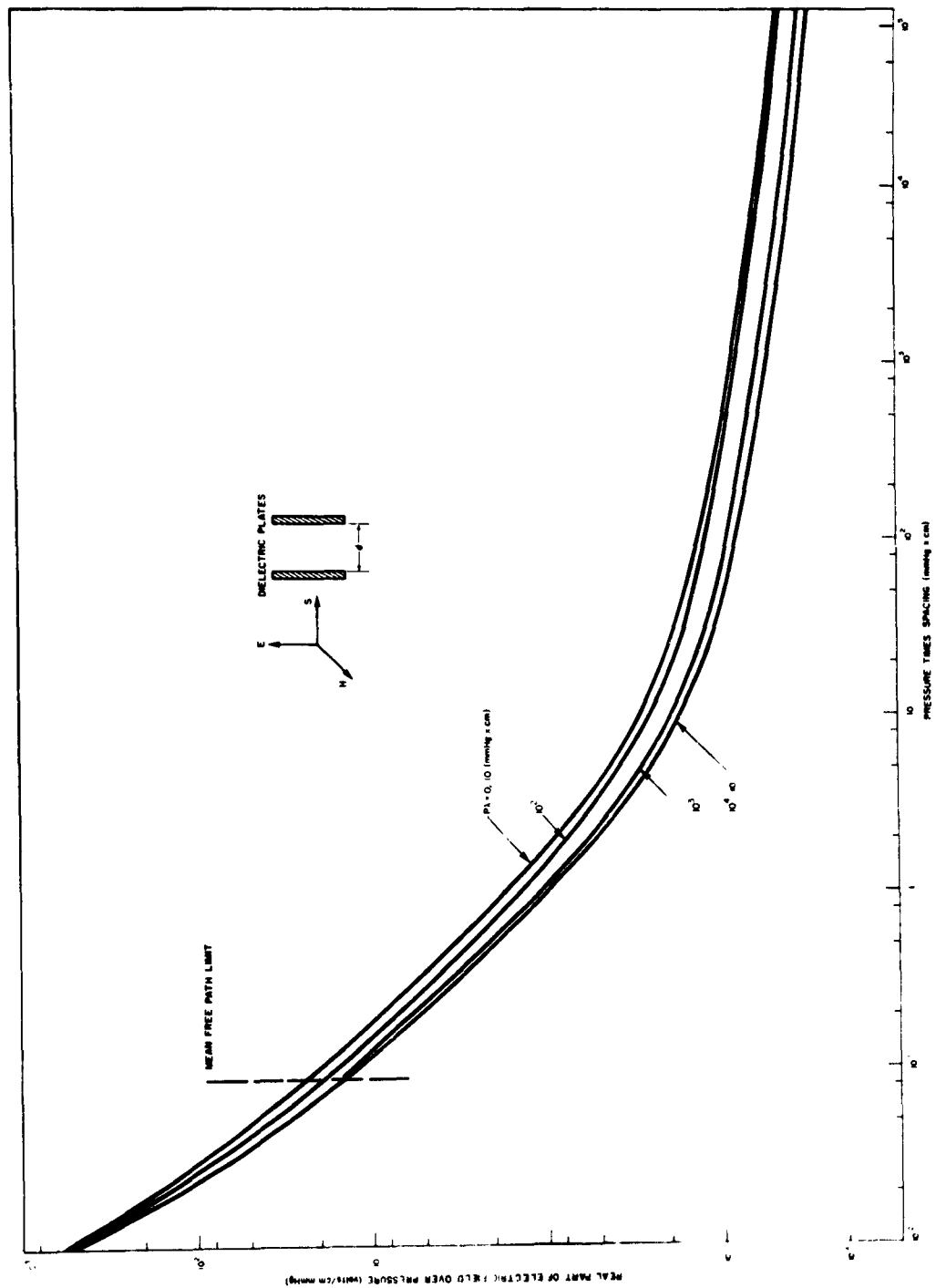


FIG. 7 Normalized Surface Resistance Versus Normalized Surface Current Density for Infinite pa



C46-547

FIG. 8 Real Component of Sustaining Field in Argon

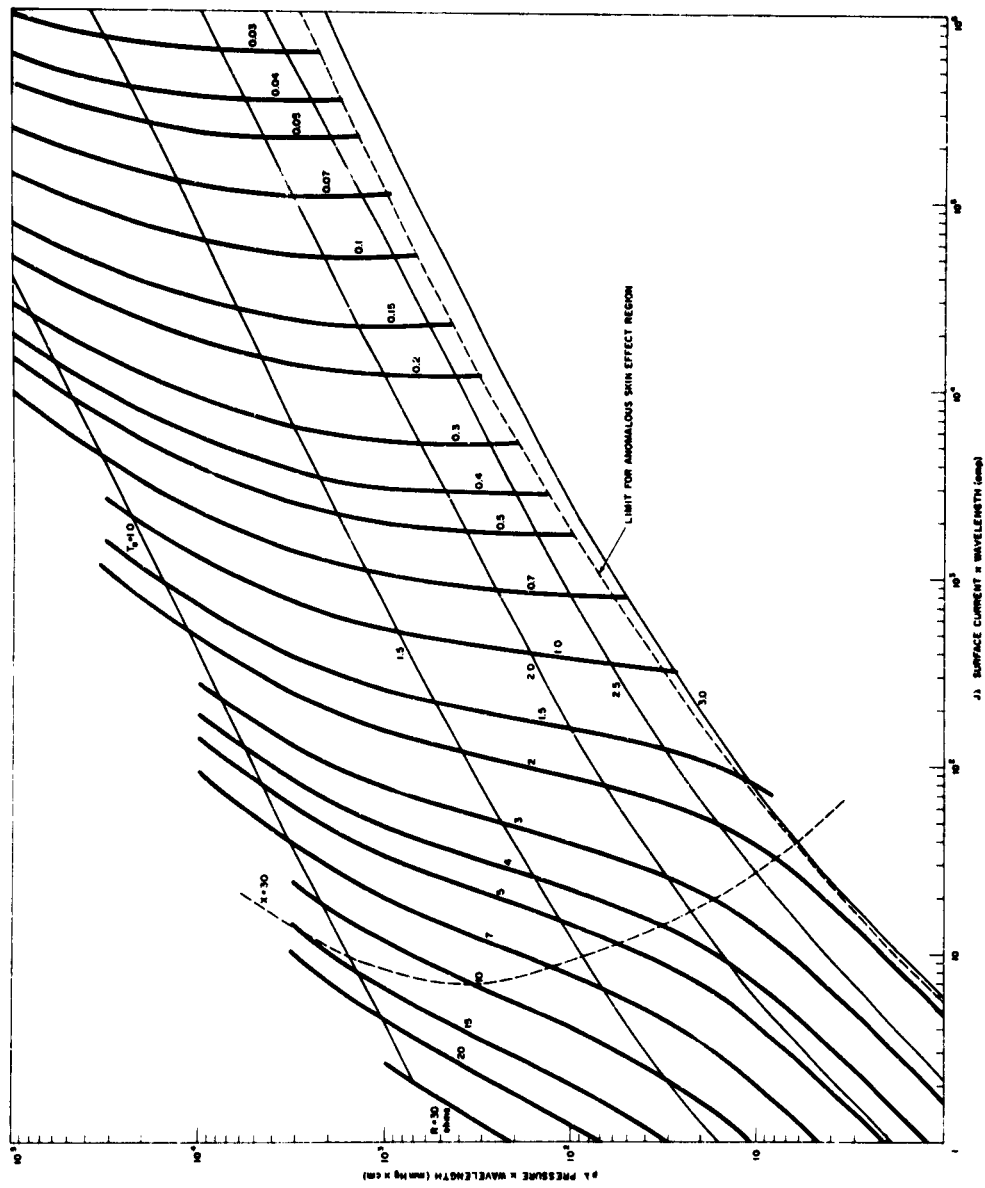
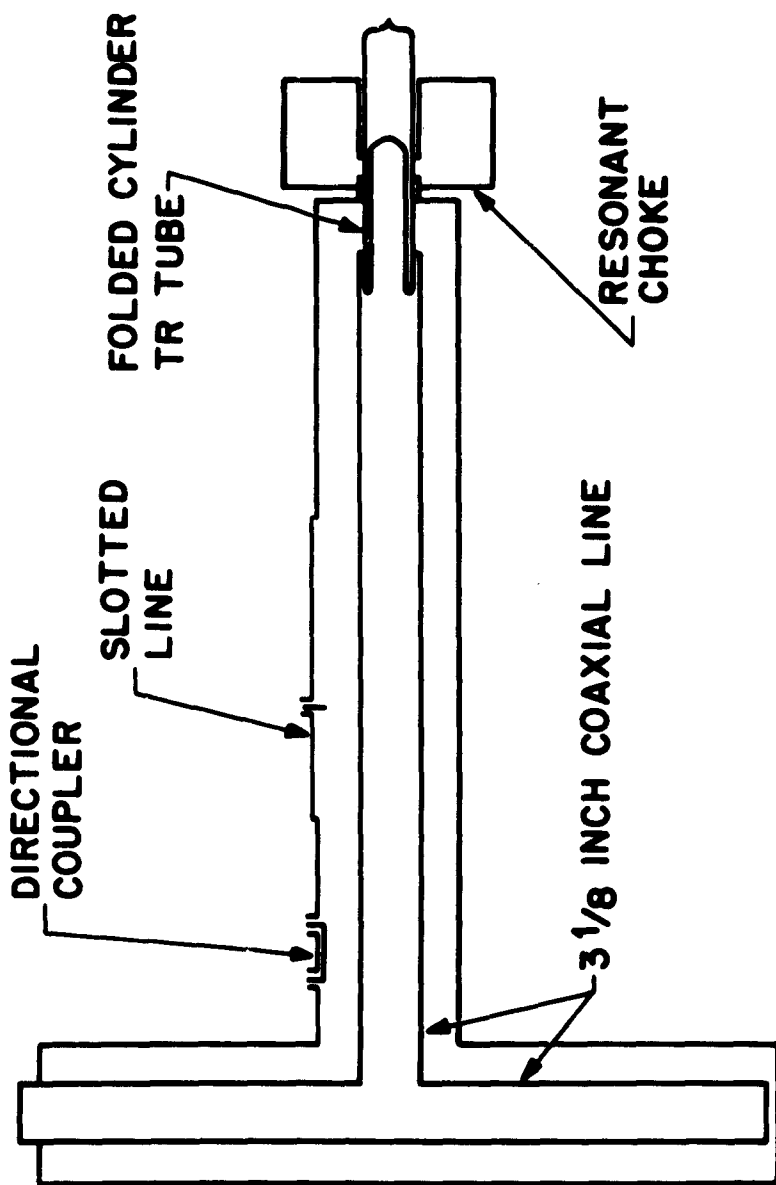


FIG. 9 Contours of Constant Surface Resistance for a Well-Shielded Discharge in Argon C46-548



ARC LOSS MEASUREMENT

C46-298

FIG. 10 Experimental Setup for Measuring Arc Loss

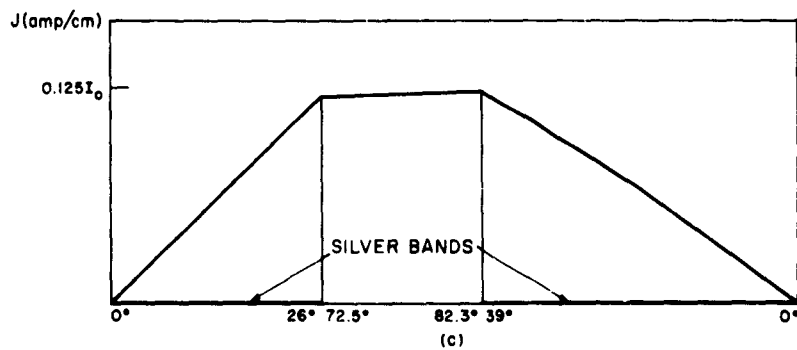
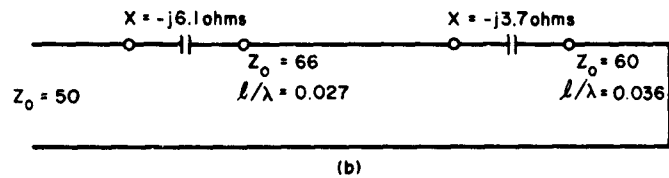
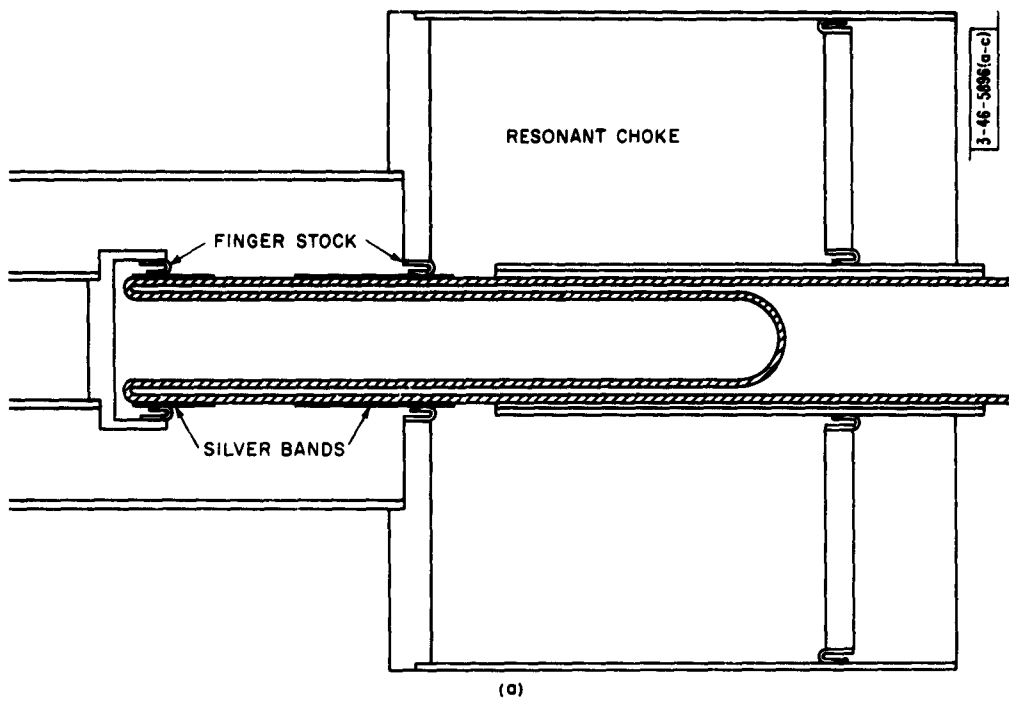


FIG. 11 (a) Details of Folded Cylinder Mount
 " 11(b) Equivalent Circuit
 " 11(c) Current Density Along Tube

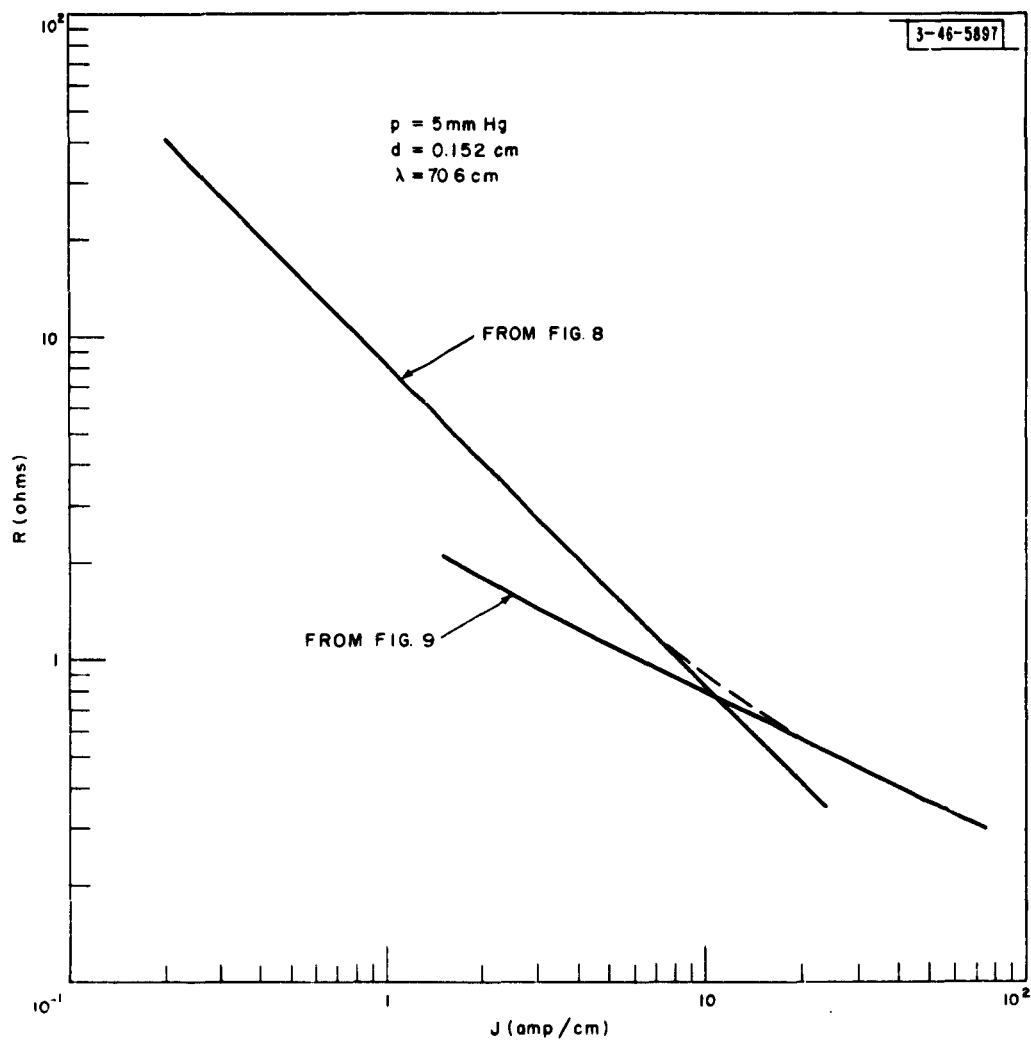


FIG. 12 Surface Resistance Versus Surface Current Density for Tube Shown in FIG. 11

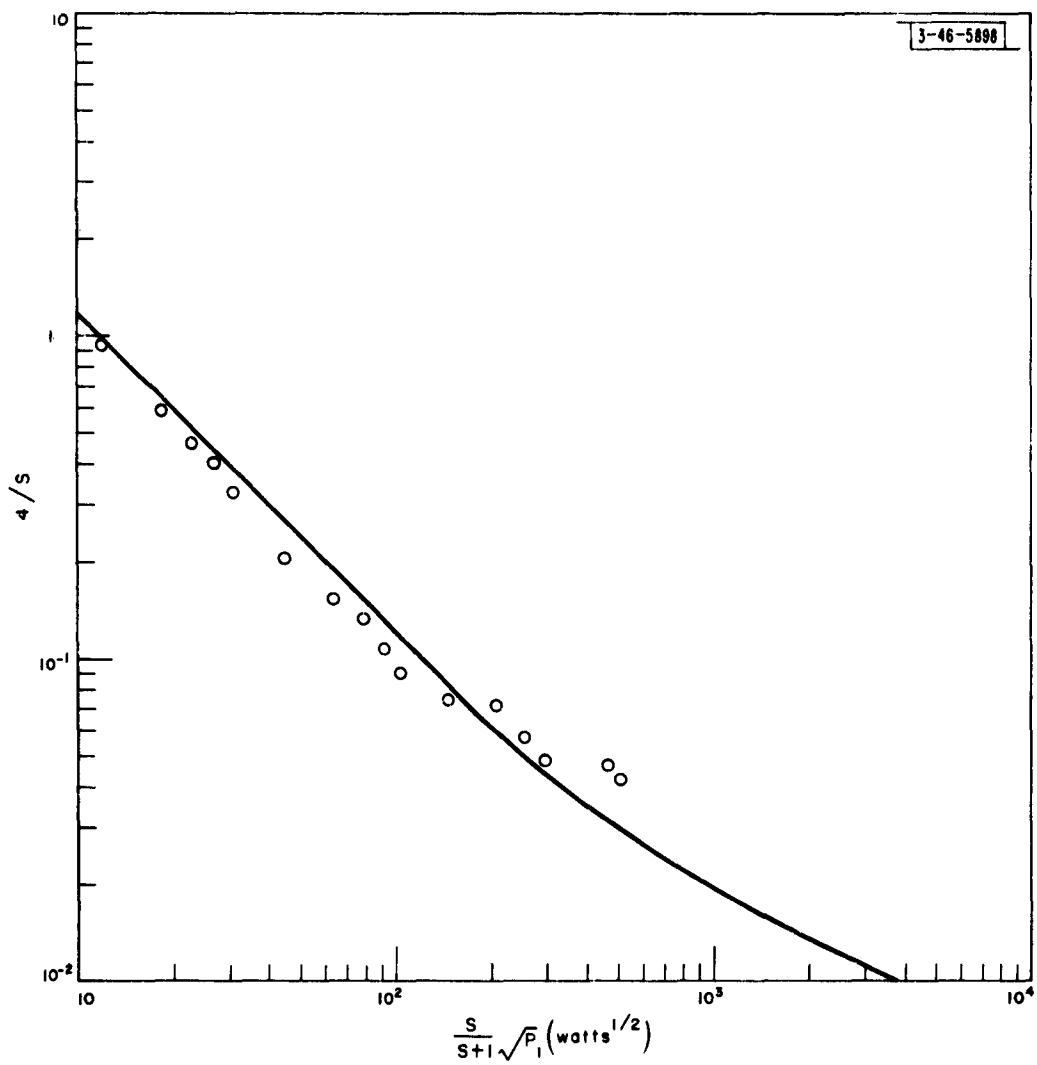


FIG. 13 Comparison of Experimental Arc Loss Measurements to Theory



FIG. 14 Folded Cylinder Mounted Perpendicular to 3 1/8-inch Coaxial Line

P400-48

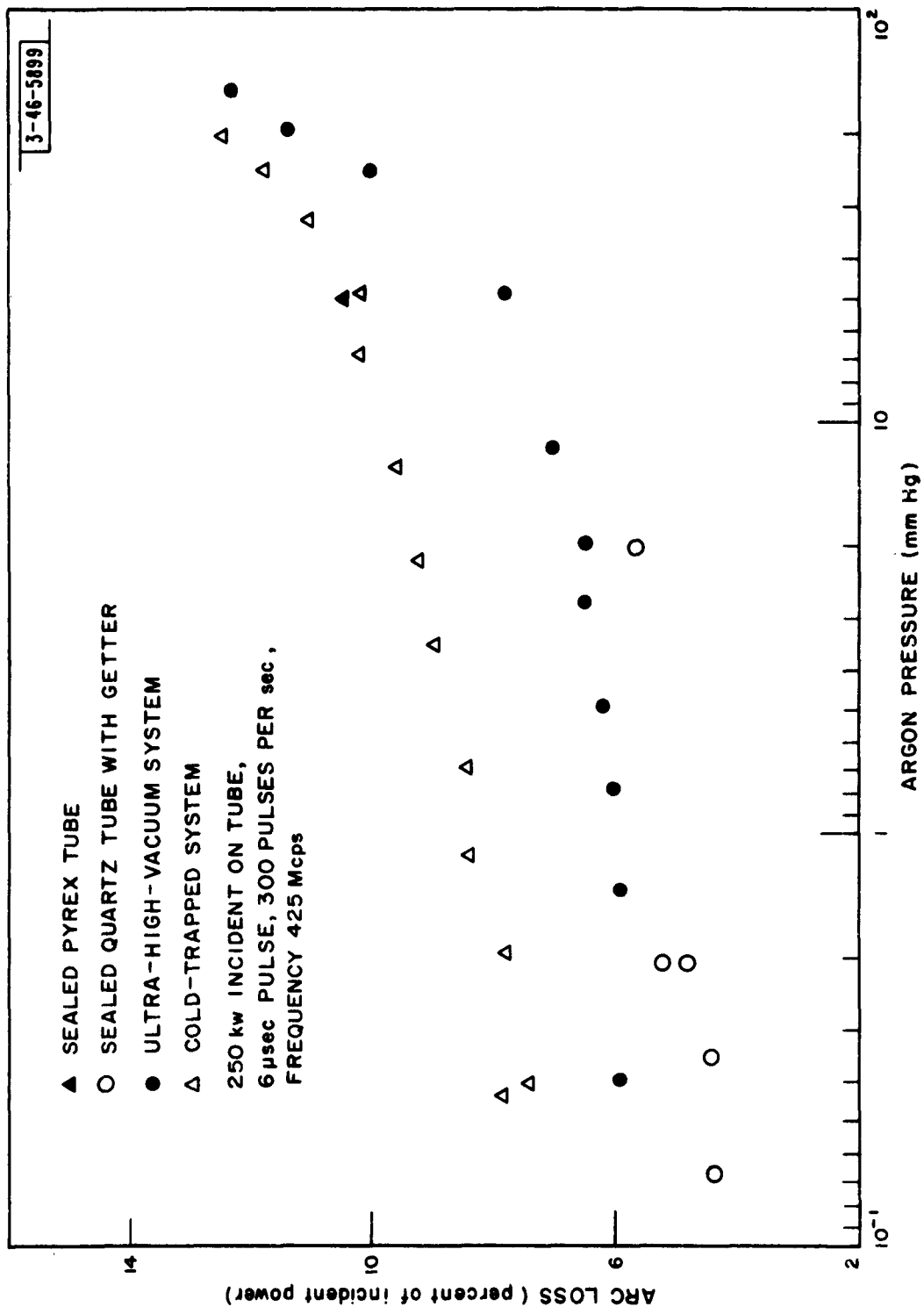


FIG. 15 Measured Arc Loss for Tube Shown in FIG. 14

APPENDIX

The d.c. positive column was first fully analyzed by Tonks and Langmuir¹¹ about 1929. At this early date practically no data existed on the probability of excitation in various gases so that a complete energy balance could not be made. About 1935, Maier-Leibnitz¹⁵ measured the excitation probability in several inert gases so that Mierdel¹⁶ could complete the analysis. Later, Waymouth and Bitter¹⁷ used somewhat the same analysis to solve the fluorescent light problem. The assumption made by all these authors is that the energy distribution among the electrons is Maxwellian. This assumption certainly is not true for vanishingly small electron densities. It has been shown by Haseltine¹⁸ and Cahn,¹⁹ however, that the electron energy distribution approaches a Maxwellian distribution if the electron density is high enough to result in a large transfer of energy among electrons of various velocities due to electron-electron collisions. Indeed, in argon if about one part in 10^5 of the gas is ionized, the distribution should approach the Maxwellian distribution:

$$f(u) = \frac{2}{T_e^{3/2}} \left(\frac{u}{\pi}\right)^{1/2} e^{-\frac{u}{T_e}} \quad (A1)$$

The ionization function is:

$$\frac{v_1}{D_a p^2} = \frac{1}{\mu_3 T_e p} \int_0^\infty P_1 \left(\frac{2e}{m} u\right)^{1/2} f(u) du \quad (A2)$$

Here we have assumed all ionizations to be direct (no cumulative ionization)($D_a = \mu_3 T_e$).⁹ The probability of ionization, P_1 , has been assumed to be directly proportional to the energy above the ionization potential, u_1 .

$$P_1 = h_1(u - u_1) \quad (A3)$$

With this approximation and performing the integration we find:

$$\frac{v_1}{D_a p^2} = \frac{h_1}{\mu_3 p} \sqrt{\frac{8e}{\pi m T_e}} (u_1 + 2T_e) e^{-\frac{u_1}{T_e}} \quad (A4)$$

The mobility of the plasma written in terms of the velocity, v , is given by:

$$\mu = -\frac{4\pi e}{3m} \int_0^\infty \frac{v^3}{v_c + j\omega} \frac{\partial f(v)}{\partial v} dv \quad (A5)$$

In terms of energy, u , this becomes:

$$\frac{\mu}{T_e} = -\frac{2}{3} \frac{e}{m T_e} \int_0^\infty \frac{u^{3/2}}{P_1 \left(\frac{2eu}{m}\right)^{1/2} + j\frac{\omega}{p}} \frac{\partial \left[\frac{f(u)}{u^{1/2}} \right]}{\partial u} du \quad (A6)$$

Substituting (A1) into (A6), we find:

$$\frac{\mu}{T_e} = \frac{2}{3T_e^{7/2}} \sqrt{\frac{2e}{\pi m}} \int_0^\infty \frac{u^{3/2} e^{-\frac{u}{T_e}}}{P_c u^{1/2} + j\sqrt{\frac{2m}{e}} \frac{\pi c}{p\lambda}} du \quad (A7)$$

To find the field necessary to sustain a discharge we must next perform an energy balance in the plasma. Consider a differentially small volume. The electrons in this volume lose energy by collisions with the gas molecules. Some collisions are elastic, some exciting and some ionizing. These energy losses are found using the next three equations.

$$\frac{W_c}{pn} = \frac{2me}{M} \int_0^\infty u P_c \left(\frac{2eu}{m}\right)^{1/2} f(u) du \quad (A8)$$

$$\frac{W_e}{pn} = eu_e \int_0^{\infty} P_e \left(\frac{2eu}{m}\right)^{1/2} f(u) du \quad (A9)$$

$$\frac{W_i}{pn} = e(u_i + \frac{3T_e}{2}) \int_0^{\infty} P_i \left(\frac{2eu}{m}\right)^{1/2} f(u) du \quad (A10)$$

Here we have used the fact that the average fractional loss of energy in an elastic collision is $\frac{2m}{M}$. For P_e we have assumed the form

$$P_e = h_e(u - u_e) \quad (A11)$$

The term $3T_e/2$ in (A10) takes care of the fact that for every ion produced an electron with average energy $\frac{3}{2}T_e$ diffused out of the small volume considered here. We have neglected two terms in the energy balance equation. They are: 1) a term that accounts for the heat flow due to any temperature gradient in the plasma; and 2) a term that accounts for the energy lost by the electrons as they diffuse against the field set up by the ambipolar diffusion¹⁰ mechanism. Fortunately, these terms are usually small compared to the other energy loss terms. We must neglect these terms because we do not know a priori the gradient in the temperature or the electric field set up by the ambipolar diffusion mechanism. It is precisely the neglect of these terms which allows us to assign an electron temperature for each E/p in the plasma.

The total energy loss is

$$\frac{W}{pn} = \frac{W_c}{pn} + \frac{W_e}{pn} + \frac{W_i}{pn}, \quad (A12)$$

and the necessary sustaining field is given by:

$$\frac{E}{p} = \left[\left(\frac{W}{pn} \right) / \left(\frac{\sigma_1 p}{n} \right) \right]^{1/2} = \left[\left(\frac{W}{pn} \right) / (\mu_1 p e) \right]^{1/2} . \quad (A13)$$

Equations (A3) to (A13) were used with the constants appearing in Table A1 and the P_c versus u curves shown in Fig. A1, together with an electronic computer to calculate the results shown in Figs. 2 through 5. The d.c. sustaining fields in a positive column calculated for argon are compared with the experimental results of Klarfeld²⁰ and Groos²¹ in Fig. A2. Here, E_a is plotted as a function of p_a . In plotting the theoretical results, we have used the fact that when the electric field and the electron temperature are constant throughout the volume of a diffusion-controlled discharge,

$$\frac{v_1}{D_a p^2} = \frac{1}{(p\lambda)^2} = \left(\frac{2.4 C_k}{p_a} \right)^2 . \quad (A14)$$

Below a pressure such that the mean-free path of the positive ions equals a diffusion length, the diffusion theory no longer holds. Instead, the ions are constantly accelerated by the space charge fields on their way to the walls. Tonks and Langmuir¹¹ have solved for the variation in charge density and radial potential in a very low pressure discharge and von Engel has shown how to calculate the electron temperature.²² Tonks and Langmuir showed that

$$v_1 = \frac{0.7722}{a} \left(\frac{2eT_e}{m_p} \right)^{1/2} \quad (A15)$$

Combining (A15) with (A2) and remembering that $D_a = \mu_3 T_e$, we find

$$pa = \frac{0.7722}{\int_0^{\infty} P_1 \left(\frac{mu}{mT_e} \right)^{1/2} f(u) du} \quad (A16)$$

We have used the exact expression rather than the approximation of (A3) because the electron temperature often exceeds the value where the approximation of (A3) is valid. The results of graphical integrations over the actual P_1 curve are shown by the dotted line of Fig. 2. The solid curve on Fig. A2 at low values of pa is a plot of (A16) and the solid curve at high pa is a result of applying (A14). It can be seen that the shape of the curve of experimental results roughly verifies the theory, having two minima and crossing over from one solution to the other at about the mean-free-path limit.

To elucidate this experimental discrepancy, we have drawn two more graphs--one of the electron temperature versus pa (Fig. A3), and one of E/P versus electron temperature (Fig. A4). Furthermore, we have corrected the energy balance equation (A10) by adding a term $5T_e$, which is the approximate energy loss that an average electron suffers in diffusing out of the discharge.¹¹ This last correction gives the dashed lines in Figs. A2 and A4. Notice that there is good agreement between theory and experiment in A4 at high electron temperatures so that our energy balance equations are probably correct. We further note that if the values of pa calculated from (A14) and (A16) could be about doubled, the experimental result, would agree quite well with theory. A critical examination of the assumptions made in deriving the (A14) and (A16) and of the experimental methods used is probably in order.

An interesting conclusion can be drawn from Fig. (A3). There is some minimum value of pa at which a discharge can be maintained. As pa decreases,

more electrons are lost by diffusion and a higher value of v_1 is required. As seen in Fig. 2, there is a maximum in the v_1 versus T_e curve so that, as p_a is reduced, eventually a point will be reached where the additional ionization cannot be produced by raising the electron temperature.

TABLE A1

Constants Used in Computation for Argon

$$\mu_e = 11.6 \text{ volts}$$

$$h_e = 0.400 \text{ (volt cm x mm Hg)}^{-1}$$

$$\mu_i = 15.8 \text{ volts}$$

$$h_i = 0.755 \text{ (volt cm x mm Hg)}^{-1}$$

$$\mu_{3p} = 1260 \text{ cm}^2 \text{ mm Hg/volt sec}$$

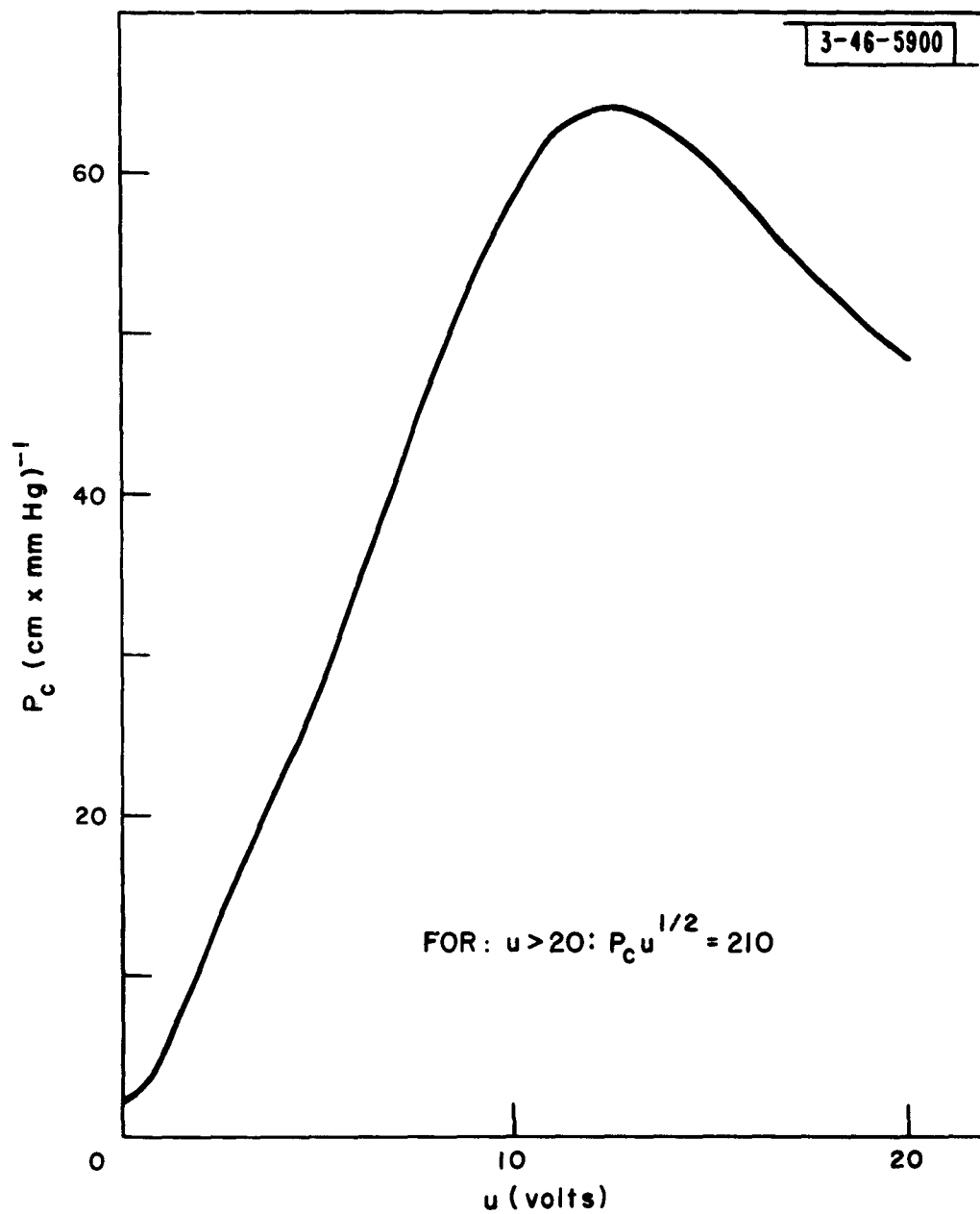


FIG. A1 Probability of Collision Values Used in Calculations

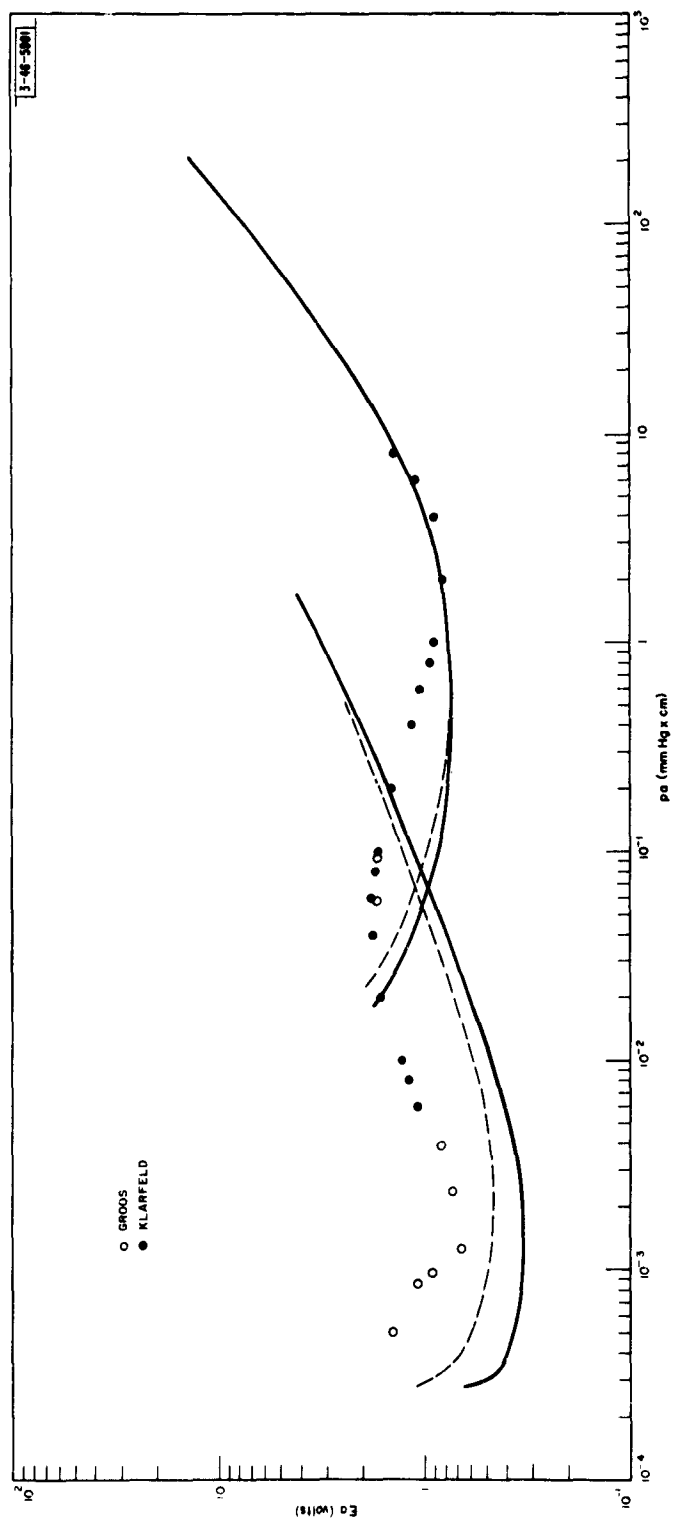


FIG. A2 Calculated and Experimental Values of E_a as a Function of p

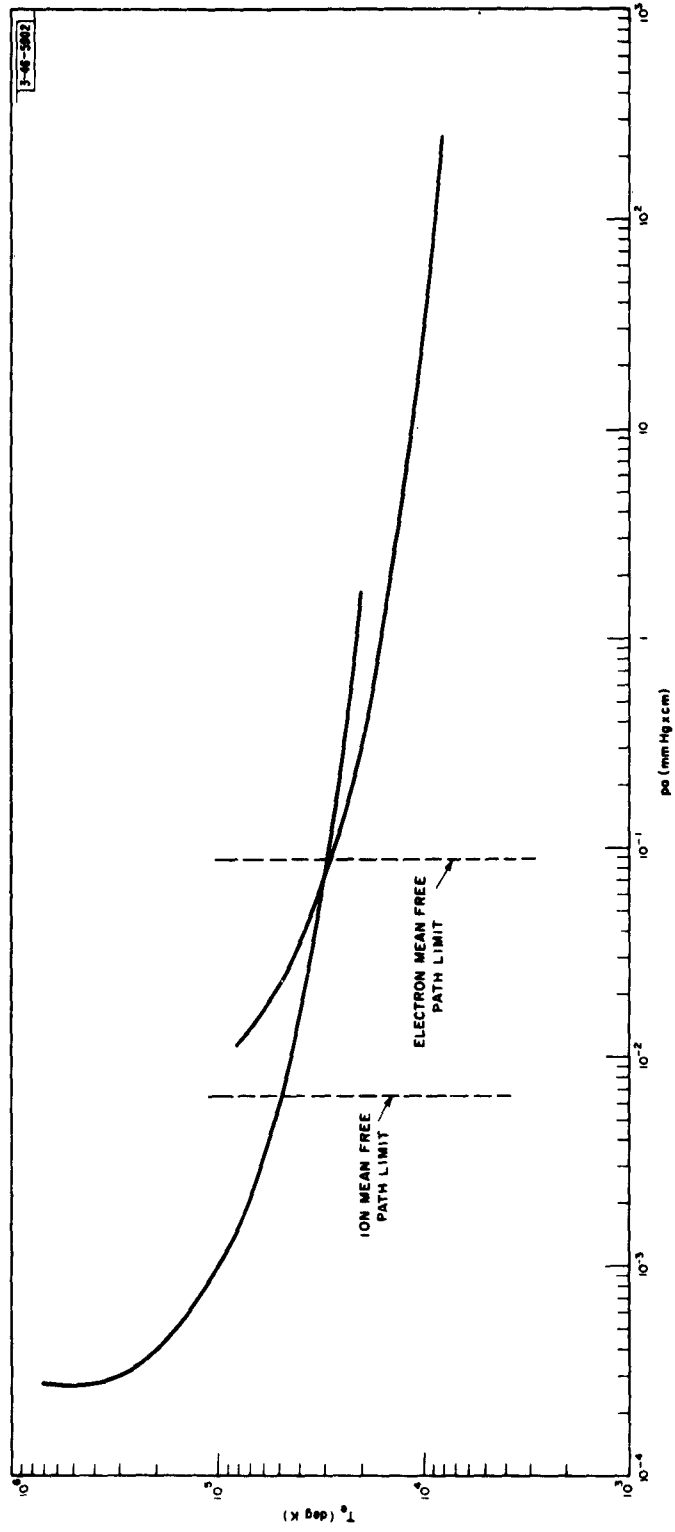


FIG. A3 Electron Temperature as a Function of p for Argon

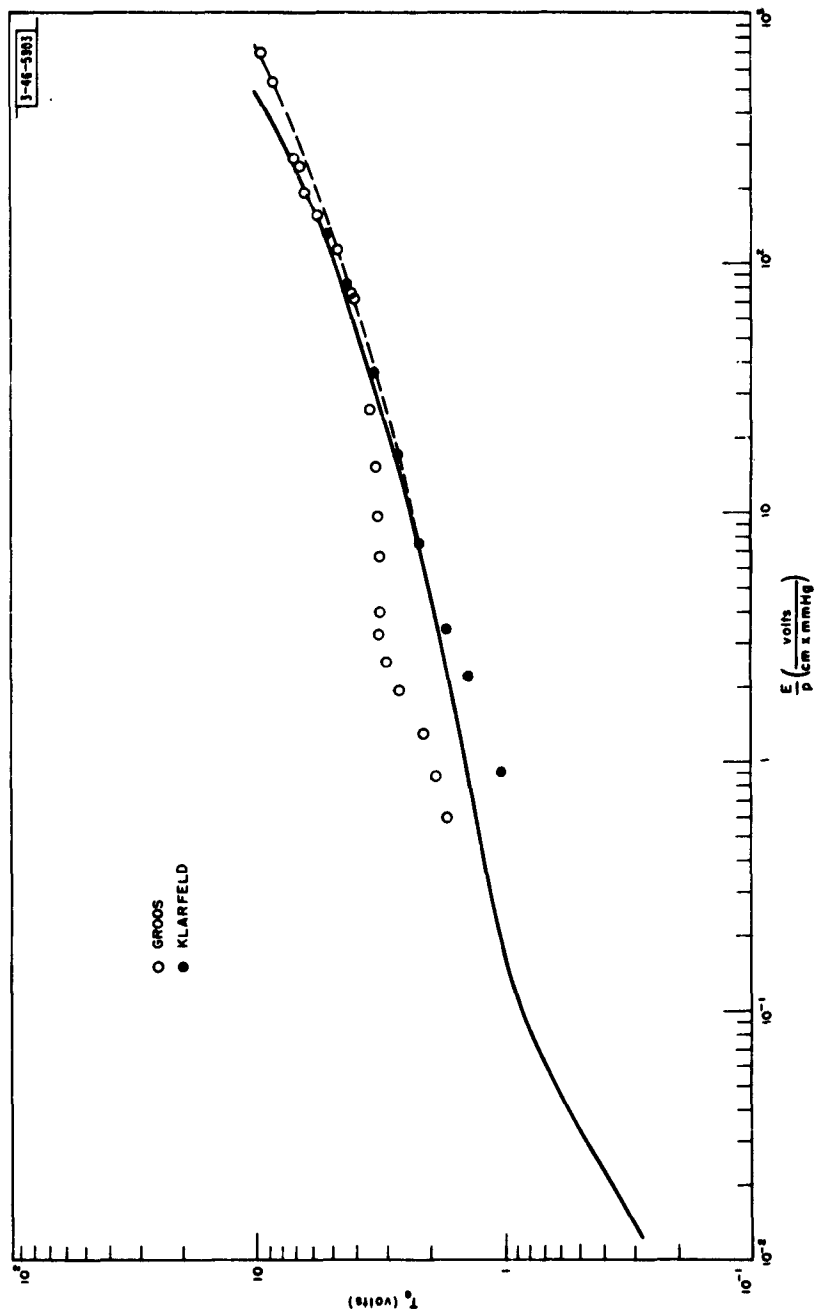


FIG. A4 Calculated and Experimental Values of Electron Temperature as a Function of E/p

REFERENCES

- 1) C. E. Muehe, "High Power Duplexers," IRE Trans., MTT-9, 506-512, (November, 1961).
- 2) L. D. Smullin and C. B. Montgomery, Microwave Duplexers, 14, Radio-Laboratory Series (McGraw-Hill, N. Y., 1948).
- 3) A. F. Harvey, "Duplexing Systems at Microwave Frequencies," IRE Trans, MTT-8, 415-431 (July, 1960).
- 4) S. Krasik, D. Alpert and A. O. McCoubrey, "Breakdown and Maintenance of Microwave Discharges in Argon," Phys. Rev., 76, 722-730 (September, 1949).
- 5) P. Johnson, "Discharges in Neon," Phil. Mag., 10, 921-931 (1930).
- 6) F. L. Jones, "High Frequency and Direct Current Discharges in Helium," Phil. Mag., 11, 163-173 (1931).
- 7) S. Kojima, K. Takayama, and A. Shimanchi, "Probe Measurements for High Frequency Discharge III," J. Phys. Soc. of Japan, 55-59 (January-February, 1953).
- 8) S. Ramo and J. R. Whinnery, Fields and Waves in Modern Radio (John Wiley and Sons, N. Y., 1953).
- 9) S. C. Brown, Basic Data of Plasma Physics, (The Technology Press of M.I.T. and John Wiley and Sons, N. Y., 1959).
- 10) W. P. Allis and D. J. Rose, "The Transition from Free to Ambipolar Diffusion," Phys. Rev., 93, 84-93 (1954).
- 11) L. Tonks and I. Langmuir, "A General Theory of the Plasma of an Arc," Phys. Rev., 34, 876-922 (1929).
- 12) G.E.H. Reuter and E. H. Sondheimer, "The Theory of Anomalous Skin Effect in Metals," Proc. Roy. Soc., A195, 336-364 (1948).
- 13) L. Spitzer, Physics of Fully Ionized Gas, (Interscience Publishers, Inc., N. Y., 1956)
- 14) G. H. Dieke and H. M. Crosswhite, "Purification of Rare Gases by Activated Uranium," Jour. Opt. Soc. of Am., 42, 433 (June, 1952).
- 15) H. Maier-Leibnitz, "Ausbeutemessungen Beim Stoss Langsamer Elektronen Mit Edelgasatomen," Zeitz. f. Phys., 95, 499-523 (1935).
- 16) G. Mierdel, "Über Die Energieumsetzung Durch Elektronenstoss in Edelgassäulen," Wiss. ver. Siemens, 17, 71-84 (1938).
- 17) J. F. Waymouth and F. Bitter, "Analysis of the Plasma of Fluorescent Lamps," J. A. P., 27, 122-131 (1956)

- 18) W. R. Haseltine, "The Mutual Interaction of Plasma Electrons," J. of Math. and Phys., 18, 174-201 (1939).
- 19) J. H. Cahn, "Electronic Interaction in Electrical Discharges in Gases," Phys. Rev., 75, 293-300 (1949). "Electron Velocity Distribution Function in High Frequency Alternating Fields Including Electronic Interactions," Phys. Rev., 75, 838-841 (1949).
- 20) B. Klarfeld, "The Potential Gradient in the Positive Column," J. Tech. Physics of U.S.S.R., 5, 725-740 (1938).
- 21) O. Groos, "Über Die Mechanismus Der Positiven Säule Der Glimmentladung In Argon," Feitz, F. Phys., 88, 741-756 (1934).
- 22) A. von Engel, Ionized Gases, (Oxford Press, London, 1955).